Molecular Crystals and Liquid Crystals

Publication details, including instructions for authors and subscription information:
http://www.tandfonline.com/loi/gmcl20

Theoretical and Computational Rheology for Discotic Nematic Liquid Crystals

Dana Grecov [a] & Alejandro D. Rey [a]

[a] Department of Chemical Engineering, McGill University, 3610 University Street, Montreal, Quebec, H3A 2B2, Canada

Version of record first published: 18 Oct 2010

To cite this article: Dana Grecov & Alejandro D. Rey (2002): Theoretical and Computational Rheology for Discotic Nematic Liquid Crystals, Molecular Crystals and Liquid Crystals, 391:1, 57-94

To link to this article: http://dx.doi.org/10.1080/10587250216174

Mol. Cryst. Liq. Cryst., Vol. 391, pp. 57–94

1542-1406/03 $12.00 + .00
DOI: 10.1080/15421400390193576

Taylor & Francis
Taylor & Francis Group

THEORETICAL AND COMPUTATIONAL RHEOLOGY FOR DISCOTIC NEMATIC LIQUID CRYSTALS

*Dana Grecov and Alejandro D. Rey**
Department of Chemical Engineering, McGill University,
3610 University Street, Montreal, Quebec H3A 2B2, Canada

This paper presents an analysis of the role of orientation on the rheology of discotic nematic liquid crystals. The shear rheological properties exhibited by flow-aligning discotic mesophases are calculated by using a complete generalized nonlinear second-order tensor Landau-de Gennes model that takes into account short-range order elasticity, long-range elasticity, and viscous effects. A unified expression for the extra stress tensor is given. The second-order tensor Landau-de Gennes model was reduced to the uniaxial Leslie-Ericksen to obtain limiting rheological material functions valid at low and high shear rates. Analytical results are able to predict the material functions computed by the full Landau-de Gennes model for nonhomogeneous flow-aligning discotic nematic liquid crystals. Experimentally reported changes in the sign of the first normal stress differences with shear rate are captured by the model. A new Carreau-Yasuda liquid crystal model has been used to characterize the shear rheology for characteristic boundary conditions, and a viscosity power law exponent of 0.5 and a normal stress coefficient power law exponent of 0.44 have been obtained.

Keywords: shear flow; flow-aligning; Lesile-Ericksen theory; discotic nematic liquid crystal; rheological properties

INTRODUCTION

Carbonaceous mesophase are discotic liquid crystalline materials, formed by disc-shaped flat aromatic molecules that are large enough to exhibit nematic ordering [1], with an average molecular weight near 2000 [2]. They possess very high axial thermal conductivity and elastic modulus and thus are very suitable for industrial processes requiring high thermal transport

Received 15 April 2002; accepted 11 September 2002.
The authors gratefully acknowledge the support for this research from the NSF Center for Advanced Fibers and Films (CAEFF/NSF) at Clemson University.
*Corresponding author. E-mail: alejandro.rey@mcgill.ca

and stiffness [3, 4]. Advances in the spinning of carbonaceous mesophases into fibers make the understanding of the flow behavior of discotic liquid crystals to be of considerable practical value.

Figure 1 shows a schematic of the uniaxial discotic nematic liquid crystal (DNLC) phase. The DNLCs consist of flat, disklike molecules more or less aligned along a common direction, represented by the uniaxial director **n** (the average orientation of the unit normals to the disklike molecules). The degree of order of the unit normals along **n** is given by the scalar order parameter S. The second order tensor order parameter $\mathbf{Q} = \mathrm{S}\,(\mathbf{nn\text{-}I}/3)$ takes into account both orientation and order. In the more general biaxial state, the tensor order parameter **Q** is given in terms of three eigenvalues $(\lambda_\mathrm{n}, \lambda_\mathrm{m}, \lambda_\mathrm{l})$ and three orthonormal eigenvectors (**n**, **m**, **l**). In contrast to rodlike nematics, in disklike nematics the largest molecular dimension is orthogonal to the director orientation, with the consequence that the very well-documented viscoelastic property ordering in rodlike nematics [5] is now reversed.

DNLCs are anisotropic viscoelastic materials, whose flow behavior can be described using the Leslie-Ericksen director **n** theory or by the Landau-de Gennes tensor order parameter **Q** theory. The orientation variable is a slow, long wave-length mode, and the scalar order parameter is a fast, short wave-length mode. Thus the selection of the theory depends on the purpose and use of the model. For fast flows and/or descriptions of short length scale phenomena such as defect nucleation, the Landau-de Gennes model must be used. For sufficiently slow flows, when the flow time scale is slower than the internal time scale such that the orientation dominates the rheology and the scalar order parameter is close to its equilibrium value, and long length scale phenomena, the Leslie-Ericksen theory is sufficient.

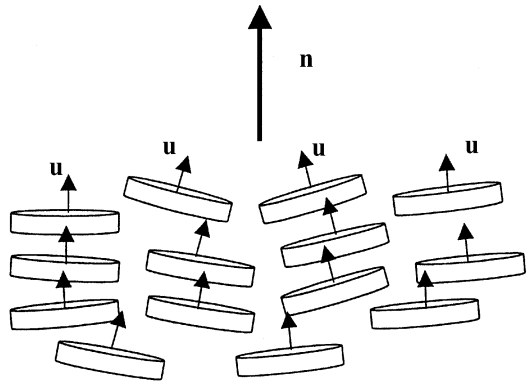

FIGURE 1 Definition of director **n** of a discotic nematic liquid crystal. The director **n** is the average director of the unit normals to the disklike molecules.

In the limit of slow flows the Landau-de Gennes theory converges with the Leslie-Ericksen theory [6], and thus the viscoelastic material parameters of the latter can be given in terms of parameters of the former. In this paper we use the dual Leslie-Ericksen vector and Landau-de Gennes tensor descriptions to extract a clear rheological characterization of DNLCs.

The shear flow behavior and rheology of DNLCs depends on the sign and magnitude of the reactive parameter λ, which is the ratio of the flow-aligning effect of the deformation rate and the tumbling (rotational) effect of the vorticity. For DNLCs it is known that $\lambda < 0$ [7]. When $\lambda < -1$, the material flow aligns close to the velocity gradient direction since the rotational effect of vorticity is overcome by deformation. When $-1 < \lambda < 0$, the director does not align close to the velocity gradient direction because the rotational effect of vorticity dominates over the aligning effect of deformation. Materials with $\lambda < -1$ display the flow-aligning mode. At present there is some evidence that carbonaceous mesophases are flow-aligning systems, since mesophase fibers show clearly ordered macroscopic orientation. It should also be mentioned that for thermotropic low molecular mass nematics the only mechanism that leads to nonaligning behavior is the proximity to the smectic A phase [8]. It has been shown that, for example, 8CB (4′-n-octyl-4-cyanobiphenyl) is a shear flow-aligning nematic at high temperatures, but as the temperature approaches the nematic-smectic A transition temperature, the material looses its ability to orient with the flow and out-of-plane orientation, and defect nucleation is likely to occur [8]. Hydroxy-propyl cellulose (HPC) in suitable solvents exhibits nonaligning behavior at low shear rates and flow-aligning behavior at high shear rates. The transition from the polymeric systems occurs at shear rates $\dot{\gamma} \approx 100\,\mathrm{s}^{-1}$ [9]. No systematic data that shows that thermotropic liquid crystals such as Vectra are nonaligning materials has been presented. At present there appears to be a consensus that thermotropic nematic polymers are flow aligning [10].

The characterization of shear material functions for melts and liquid crystals includes the steady shear viscosity and the first normal stress difference. As mentioned above, for slow flows the orientation dominates the process, while for fast flows the order parameter process must be taken into account. Orientation-dominated processes include flow-induced orientation, boundary layers, and textural transformations and occur when the flow time scale is faster than the orientation time scale. Order parameter flow processes include defect nucleation, nonequilibrium phase transitions, and flow-induced order parameter modifications. To access order parameters processes the flow time scale has to be faster than the order parameter time scale. This article is restricted to orientation flow processes where the flow time scale is always slower than the order parameter time scale.

Low molar nematic liquid crystals display shear thinning and thickening viscosity behavior [1, 8, 10], even in the absence of defects, driven by overall orientation changes. Here we show under what conditions is shear thinning or thickening in DNLCs likely to occur. The first normal stress difference has been well characterized for nonaligning lyotropic cholesteric polymers such as HPC and shows positive to negative to positive sign changes as the shear rate increases [10]. It is currently accepted that these sign changes in lyotropic nematic polymers are evidence of the nonaligning behavior at low shear rates and aligning behavior at higher shear rates, driven by order parameter processes. For flow-aligning low molecular weight liquid crystals, in accordence with experimental results given by [24], the steady shear viscosity exhibits shear thinning with a slope of $-1/2$, then a plateau region is reached. The first normal stress difference exhibits a negative value at low shear rates and becomes positive at higher shear rates.

In this paper we characterize the first normal stress difference of flow-aligning DNLCs and show that even flow-aligning systems show sign changes, as already predicted by Currie for rodlike nematics [11] and solely driven by orientation processes.

The particular objectives of the article are: (1) characterize the steady shear rheological material functions of flow-aligning DNLCs, and (2) elucidate the specific role of the underlying disklike geometry on the rheology of flow-aligning DNLCs.

This article aims at describing the rheology of a representative thermotropic discotic nematic liquid crystal that aligns under weak shear flows with the average molecules unit normal close to the velocity gradient directions. Other types of liquid crystals, other flow types, and other flow conditions are outside the scope of this article. Generalizations to other material systems and flow conditions will require special considerations to the material parameters appearing in the constitutive equations.

The organization of this article is as follows: In the next section we present the governing equations that describe the microstructure for discotic nematics under arbitrary flow. In the following section a unified expression for the extra stress tensor is given. In the next section we present the mapping between our tensor Landau-de Gennes theory and L-E Theory. In the section "Viscosities Coefficients Selection Procedure," we present and use several criteria to determine the material parameters. In the following section we show theoretical values of first normal stress difference and show that there are sign transitions. In the section "Selected Computational Results," we present the computational flow geometry, the boundary conditions, and initial conditions used to compute the rheological properties (first normal stress difference and apparent shear viscosity) and the shear-induced microstructure. Finally, in the last section conclusions are given.

CONSTITUTIVE EQUATIONS

The microstructure of DNLCs is described conveniently in terms of a second-order, symmetric and traceless tensor order parameter **Q** [12]:

$$\mathbf{Q} = \int \left(\mathbf{uu} - \frac{\mathbf{I}}{3} \right) f \, d^2\mathbf{u} \tag{1}$$

where **u** is the unit vector normal to the disklike molecules (see Figure 1), **I** is second-order unit tensor, and f is the orientation distribution function. Alternatively, **Q** can also be defined in terms of three eigenvectors (**n**, **m**, and **l**) and three eigenvalues (λ_n, λ_m, and λ_l):

$$\mathbf{Q} = \lambda_n \mathbf{nn} + \lambda_m \mathbf{mm} + \lambda_l \mathbf{ll} \tag{2}$$

The eigenvalues can be presented as functions of the scalar order parameter S and the biaxial order parameter P [13]:

$$\lambda_n = \frac{2}{3}\mathrm{S}, \quad \lambda_m = \frac{1}{3}(\mathrm{P} - \mathrm{S}), \quad \lambda_l = -\frac{1}{3}(\mathrm{P} + \mathrm{S}) \tag{3}$$

with the restriction

$$\lambda_n + \lambda_m + \lambda_l = 0 \tag{4}$$

The governing equations for liquid crystal flows follow from the dissipation function Δ:

$$\Delta = \mathbf{t}^s : \mathbf{A} + \mathrm{ckT}\mathbf{H} \cdot \hat{\mathbf{Q}} \tag{5}$$

where $\mathbf{t}^s$ is the viscoelastic stress tensor, c is the concentration of molecules per unit volume, k is the Boltzmann constant, T is the absolute temperature, **A** is the symmetric traceless rate of deformation tensor, **H** is the molecular field, and $\hat{\mathbf{Q}}$ is the Jaumann derivative of the tensor order parameter, given by

$$\begin{aligned} &(a)\mathbf{A} = \frac{1}{2}\left(\nabla\mathbf{v} + \nabla\mathbf{v}^{\mathrm{T}}\right); \; (c)\hat{\mathbf{Q}} = \frac{\partial \mathbf{Q}}{\partial t} + (\mathbf{v}\cdot\nabla)\mathbf{Q} - \mathbf{W}\cdot\mathbf{Q} + \mathbf{Q}\cdot\mathbf{W}; \\ &(b)\mathbf{W} = \frac{1}{2}\left(\nabla\mathbf{v} - \nabla\mathbf{v}^{\mathrm{T}}\right); \; (d)(\mathrm{ckT})\mathbf{H} = -\left[\frac{\delta F}{\delta \mathbf{Q}}\right]^{[s]} = \left[\frac{\partial f}{\partial \mathbf{Q}} - \nabla \cdot \frac{\partial f}{\partial \nabla \mathbf{Q}}\right]^{[s]} \end{aligned} \tag{6a,b,c,d}$$

where F is the total free energy and f is the free energy density:

$$\begin{aligned} \mathrm{f} = (\mathrm{ckT}) \Bigg[&\frac{1}{2}\left(1 - \frac{1}{3}\mathrm{U}\right)\mathbf{Q} : \mathbf{Q} - \frac{1}{3}\mathrm{U}\mathbf{Q} : (\mathbf{Q}\cdot\mathbf{Q}) + \frac{1}{4}\mathrm{U}(\mathbf{Q}:\mathbf{Q})^2 \\ &+ \frac{\mathrm{L}_1}{2\mathrm{ckT}}\{\nabla\mathbf{Q} : (\nabla\mathbf{Q})^{\mathrm{T}}\} + \frac{\mathrm{L}_2}{2\mathrm{ckT}}(\nabla\cdot\mathbf{Q})\cdot(\nabla\cdot\mathbf{Q}) \Bigg] \end{aligned} \tag{7}$$

$\mathrm{U} = 3\mathrm{T}^*/\mathrm{T}$ is the nematic potential, T* is the isotropic-nematic transition temperature, L_1 and L_2 are the Landau coefficients, and the superscript [s]

denotes symmetric and traceless. Using the Landau-de Gennes free energy density, the molecular field is given by

$$-\left[\frac{\delta \mathbf{F}}{\delta \mathbf{Q}}\right]^{[s]} = (\mathrm{ckT})\mathbf{H} = -(\mathrm{ckT})\left[\left(1-\frac{1}{3}\mathrm{U}\right)\mathbf{Q} - \mathrm{U}\mathbf{Q}\cdot\mathbf{Q} + \mathrm{U}\left\{(\mathbf{Q}:\mathbf{Q})\mathbf{Q} + \frac{1}{3}(\mathbf{Q}:\mathbf{Q})\mathbf{I}\right\}\right] + (\mathrm{ckT})\left[\frac{\mathrm{L}_1}{\mathrm{ckT}}\nabla^2\mathbf{Q} + \frac{1}{2}\frac{\mathrm{L}_2}{\mathrm{c}\kappa\mathrm{T}}\left[\nabla(\nabla\cdot\mathbf{Q}) + \{\nabla(\nabla\cdot\mathbf{Q})\}^{\mathrm{T}} - \frac{2}{3}\mathrm{tr}\{\nabla(\nabla\cdot\mathbf{Q})\}\mathbf{I}\right]\right] \tag{8}$$

and contains short-range and long-range contributions. Expanding the forces ($\mathbf{t}^{\mathrm{s}}$, $\hat{\mathbf{Q}}$) in terms of fluxes ($\mathbf{A}$, ckT$\mathbf{H}$), and taking into account thermodynamic restrictions and the symmetry and tracelessness of the forces and fluxes, we can obtain the equation for $\mathbf{t}^{\mathrm{s}}$ and $\hat{\mathbf{Q}}$. The dynamics of the tensor order parameter are given by the following sum of flow $\mathbf{F}$, short-range $\mathbf{H}^{\mathrm{sr}}$, and long range $\mathbf{H}^{\mathrm{lr}}$ contributions [14]:

$$\hat{\mathbf{Q}} = \mathbf{F}(\mathbf{Q}, \nabla\mathbf{v}) + \mathbf{H}; \quad \mathbf{H} = \mathbf{H}^{\mathrm{sr}}\left(\mathbf{Q}, \bar{\mathrm{D}}_{\mathrm{r}}(\mathbf{Q})\right) + \mathbf{H}^{\mathrm{lr}}(\nabla\mathbf{Q}) \tag{9}$$

1. flow contribution $\mathbf{F}$:

$$\mathbf{F}(\mathbf{Q}, \nabla\mathbf{v}) = \frac{2}{3}\beta\mathbf{A} + \beta\left[\mathbf{A}\cdot\mathbf{Q} + \mathbf{Q}\cdot\mathbf{A} - \frac{2}{3}(\mathbf{A}:\mathbf{Q})\mathbf{I}\right] - \frac{1}{2}\beta[(\mathbf{A}:\mathbf{Q})\mathbf{Q} + \mathbf{A}\cdot\mathbf{Q}\cdot\mathbf{Q} + \mathbf{Q}\cdot\mathbf{A}\cdot\mathbf{Q} + \mathbf{Q}\cdot\mathbf{Q}\cdot\mathbf{A} - \{(\mathbf{Q}\cdot\mathbf{Q}):\mathbf{A}\}\mathbf{I}] \tag{10}$$

2. short-range elastic contribution $\mathbf{H}^{\mathrm{sr}}$:

$$\mathbf{H}^{\mathrm{sr}}\left(\mathbf{Q}, \bar{\mathrm{D}}_{\mathrm{r}}(\mathbf{Q})\right) = -6\bar{\mathrm{D}}_r\left[\left(1-\frac{1}{3}\mathrm{U}\right)\mathbf{Q} - \mathrm{U}\mathbf{Q}\cdot\mathbf{Q} + \mathrm{U}\left\{(\mathbf{Q}:\mathbf{Q})\mathbf{Q} + \frac{1}{3}(\mathbf{Q}:\mathbf{Q})\mathbf{I}\right\}\right] \tag{11}$$

3. long-range elastic contribution $\mathbf{H}^{\mathrm{lr}}$:

$$\mathbf{H}^{\mathrm{lr}}(\mathbf{Q}) = 6\bar{\mathrm{D}}_{\mathrm{r}}\left[\frac{\mathrm{L}_1}{\mathrm{c}\kappa\mathrm{T}}\nabla^2\mathbf{Q} + \frac{1}{2}\frac{\mathrm{L}_2}{\mathrm{c}\kappa\mathrm{T}}[\nabla(\nabla\cdot\mathbf{Q}) + \{\nabla(\nabla\cdot\mathbf{Q})\}^{\mathrm{T}} - \frac{2}{3}\mathrm{tr}\{\nabla(\nabla\cdot\mathbf{Q})\}\mathbf{I}]\right] \tag{12}$$

$$\bar{\mathrm{D}}_{\mathrm{r}} = \frac{\mathrm{D}_{\mathrm{r}}}{\left(1-\frac{3}{2}\mathbf{Q}:\mathbf{Q}\right)} \tag{13}$$

where $\bar{D}_r$ is the microstructure-dependent rotational diffusivity, D_r is the preaveraged rotational diffusivity (here taken to be constant), and β is the thermodynamic parameter which is not determined by molecular shape since our model contains no specific molecular information.

The dimensionless form of the governing equation for the tensor order parameter $\mathbf{Q}$ is:

$$\begin{aligned}
\mathrm{Er}\hat{\mathbf{Q}}^* = \mathrm{Er}\Bigg[&\frac{2}{3}\beta\mathbf{A}^* + \beta\Big[\mathbf{A}^*\cdot\mathbf{Q} + \mathbf{Q}\cdot\mathbf{A}^* - \frac{2}{3}(\mathbf{A}^*:\mathbf{Q})\mathbf{I}\Big] \\
&-\frac{1}{2}\beta[(\mathbf{A}^*:\mathbf{Q})\mathbf{Q} + \mathbf{A}^*\cdot\mathbf{Q}\cdot\mathbf{Q} \\
&+\mathbf{Q}\cdot\mathbf{A}^*\cdot\mathbf{Q} + \mathbf{Q}\cdot\mathbf{Q}\cdot\mathbf{A}^* - \{(\mathbf{Q}\cdot\mathbf{Q}:\mathbf{A}^*\}\mathbf{I}]\Big] \\
&-\frac{3}{\mathrm{U}}\cdot\frac{\mathrm{R}}{\left(1-\frac{3}{2}\mathbf{Q}:\mathbf{Q}\right)^2}\left[\left(1-\frac{1}{3}\mathrm{U}\right)\mathbf{Q} - \mathrm{U}\mathbf{Q}\cdot\mathbf{Q}\right. \\
&\left.+\mathrm{U}\left\{(\mathbf{Q}:\mathbf{Q})\mathbf{Q} + \frac{1}{3}(\mathbf{Q}:\mathbf{Q})\mathbf{I}\right\}\right] + \frac{3}{\left(1-\frac{3}{2}\mathbf{Q}:\mathbf{Q}\right)^2}\Big[\nabla^{*^2}\mathbf{Q}. \\
&+\frac{1}{2}\mathrm{L}_2^*[\nabla^*(\nabla^*\cdot\mathbf{Q}) + \{\nabla^*(\nabla^*\cdot\mathbf{Q})\}^{\mathrm{T}} - \frac{2}{3}\mathrm{tr}\{\nabla^*(\nabla^*\cdot\mathbf{Q})\}\mathbf{I}]\Bigg]
\end{aligned} \tag{14}$$

$$\mathrm{t}^* = \dot{\gamma}\mathrm{t}, \quad \mathbf{A}^* = \frac{\mathbf{A}}{\dot{\gamma}}, \quad \mathbf{W}^* = \frac{\mathbf{W}}{\dot{\gamma}}, \quad \nabla^* = H\nabla, \quad \mathrm{L}_2^* = \frac{\mathrm{L}_2}{\mathrm{L}_1} \tag{15}$$

where the star superscript denotes dimensionless quantities and $\dot{\gamma}$ is the characteristic shear rate. The dimensionless numbers Er (Ericksen number) and energy ratio R [6] are given by

$$\mathrm{Er} = \frac{\dot{\gamma}\mathrm{H}^2\mathrm{ckT}^*}{2\mathrm{L}_1\mathrm{D}_r} \quad \mathrm{R} = \frac{3\mathrm{H}^2\mathrm{ckT}^*}{\mathrm{L}_1} \tag{16a, b}$$

and give the ratio of viscous flow effects to long-range order elasticity, and short-range order elasticity to long-range order elasticity, respectively. The external ℓ_e and internal ℓ_i length scales of model are ordered as follows:

$$\ell_e = \mathbf{H}, \quad \ell_i = \sqrt{\frac{\mathrm{L}_1}{\mathrm{ckT}^*}}, \quad \ell_e \gg \ell_i \tag{17}$$

The external length scale describes long-scale orientation variations and the internal length scale describes short-scale order parameter variations,

such as in a defect core. The external τ_e and internal τ_i time scales of model are ordered as follows:

$$\tau_e = \frac{ckT^*H^2}{2D_rL_1}, \quad \tau_i = \frac{1}{D_r}, \quad \tau_e \gg \tau_i \tag{18}$$

The external time scale describes slow describes slow scale orientation variations, and the internal length scale describes fast scale order parameter variations, such as in a defect core. The regime of interest in this paper is when the flow time scale is slower than the internal time scale,

$$\tau_e > \frac{1}{\dot{\gamma}} \gg \tau_i \tag{19}$$

such that orientation process dominate the rheology, and the scalar order parameter is close to its equilibrium value. The relation between the time scales and the dimensionless numbers are:

$$Er = \dot{\gamma}\tau_e \quad R = \frac{6\tau_e}{\tau_i} \tag{20}$$

and orientation-dominated rheology occurs when $R \gg Er$. In this paper $R_{max} = 10^5$ and $Er_{max} = 10^5$.

TOTAL EXTRA STRESS TENSOR EQUATION

The total extra stress tensor $\mathbf{t}^t$ for liquid crystalline materials is given by the sum of symmetric viscoelastic stress tensor $\mathbf{t}^s$, antisymmetric stress tensor, and Ericksen stress tensor $\mathbf{t}^{Er}$ [13,15]:

$$\mathbf{t}^t = \mathbf{t}^s + \mathbf{t}^a + \mathbf{t}^{Er} \tag{21}$$

The symmetric visco-elastic stress tensor $\mathbf{t}^s$ is expressed as a sum of a symmetric viscous stress contribution $\mathbf{t}^v$ and an elastic stress contribution $\mathbf{t}^e$[12, 13, 16] as

$$\mathbf{t}^s = \mathbf{t}^v + \mathbf{t}^e \tag{22}$$

and obtained using the dissipation expansion in Equation (5). The stress contribution $\mathbf{t}^v$ found is given by

$$\begin{aligned}\mathbf{t}^v = {} & \nu_1\mathbf{A} + \nu_2\left\{\mathbf{Q}\cdot\mathbf{A} + \mathbf{A}\cdot\mathbf{Q} - \frac{2}{3}(\mathbf{Q}:\mathbf{A})\mathbf{I}\right\} + \nu_4[(\mathbf{A}:\mathbf{Q})\mathbf{Q} + \mathbf{A}\cdot\mathbf{Q}\cdot\mathbf{Q} \\ & + \mathbf{Q}\cdot\mathbf{A}\cdot\mathbf{Q} + \mathbf{Q}\cdot\mathbf{Q}\cdot\mathbf{A} + \{(\mathbf{Q}\cdot\mathbf{Q}):\mathbf{A}\}\mathbf{I}]\end{aligned} \tag{23}$$

where ν_1, ν_2, and ν_4 are viscosities coefficients. Characteristic values for the viscosities coefficients for DNLCs will be found by mapping the total

stress tensor with the stress tensor given by the Leslie-Ericksen vector theory (section 4). The elastic contribution $\mathbf{t}^{e}$ that couples stress to the molecular field $\mathbf{H}$ is given as:

$$\mathbf{t}^{e} = (\mathrm{ckT})\left[-\frac{2}{3}\beta\mathbf{H} - \beta\left\{\mathbf{H}\cdot\mathbf{Q} + \mathbf{Q}\cdot\mathbf{H} - \frac{2}{3}(\mathbf{H}:\mathbf{Q})\mathbf{I}\right\} + \frac{1}{2}\beta[(\mathbf{H}:\mathbf{Q})\mathbf{Q} + \mathbf{H}\cdot\mathbf{Q}\cdot\mathbf{Q} + \mathbf{Q}\cdot\mathbf{H}\cdot\mathbf{Q} + \mathbf{Q}\cdot\mathbf{Q}\cdot\mathbf{H} - \{(\mathbf{Q}\cdot\mathbf{Q}):\mathbf{H}\}\mathbf{I}]\right] \tag{24}$$

The antisymmetric contribution $\mathbf{t}^{a}$ arises whenever $\mathbf{H}\cdot\mathbf{Q}$ is not symmetric and is given as [17,18]

$$\mathbf{t}^{a} = \mathrm{ckT}(\mathbf{H}\cdot\mathbf{Q} - \mathbf{Q}\cdot\mathbf{H}) \tag{25}$$

The Ericksen stress contribution $\mathbf{t}^{\mathrm{Er}}$ arises from the long-range elasticity and is given as [18]

$$\mathbf{t}^{\mathrm{Er}} = -\frac{\partial \mathrm{f}}{\partial\nabla\mathbf{Q}} : (\nabla\mathbf{Q})^{\mathrm{T}} = \left[-\mathrm{L}_1\nabla\mathbf{Q} : (\nabla\mathbf{Q})^{\mathrm{T}} - \mathrm{L}_2(\nabla\cdot\mathbf{Q})\cdot(\nabla\cdot\mathbf{Q})^{\mathrm{T}}\right] \tag{26}$$

Summing up all the contributions and nondimensionalizing ($\mathbf{H}$ is already nondimensional):

$$\begin{aligned}\tilde{\mathbf{t}}^{\mathrm{t}} = {} & \frac{\mathrm{Er}}{\mathrm{R}}\left(v_1^*\mathbf{A}^* + v_2^*\left\{\mathbf{Q}\cdot\mathbf{A}^* + \mathbf{A}^*\cdot\mathbf{Q} - \frac{2}{3}(\mathbf{Q}:\mathbf{A}^*)\mathbf{I}\right\} + v_4^*[(\mathbf{A}^*:\mathbf{Q})\mathbf{Q}\right. \\ & \left. + \mathbf{A}^*\cdot\mathbf{Q}\cdot\mathbf{Q} + \mathbf{Q}\cdot\mathbf{A}^*\cdot\mathbf{Q} + \mathbf{Q}\cdot\mathbf{Q}\cdot\mathbf{A}^*. - \{(\mathbf{Q}\cdot\mathbf{Q}):\mathbf{A}^*\}\mathbf{I}]\right) \\ & + \frac{3}{\mathrm{U}}\left[-\frac{2}{3}\beta\mathbf{H} - \beta\left\{\mathbf{H}\cdot\mathbf{Q} + \mathbf{Q}\cdot\mathbf{H} - \frac{2}{3}(\mathbf{H}:\mathbf{Q})\mathbf{I}\right\}\right] \\ & + \frac{3}{2\mathrm{U}}\beta[(\mathbf{H}:\mathbf{Q})\mathbf{Q} + \mathbf{H}\cdot\mathbf{Q}\cdot\mathbf{Q} + \mathbf{Q}\cdot\mathbf{H}\cdot\mathbf{Q} + \mathbf{Q}\cdot\mathbf{Q}\cdot\mathbf{H} \\ & - \{(\mathbf{Q}\cdot\mathbf{Q}):\mathbf{H}\}\mathbf{I}] \\ & + \frac{3}{\mathrm{U}}(\mathbf{H}\cdot\mathbf{Q} - \mathbf{Q}\cdot\mathbf{H}) + \frac{3}{\mathrm{R}}\left[-\nabla^*\mathbf{Q} : (\nabla^*\mathbf{Q})^{\mathrm{T}} - \frac{\mathrm{L}_2}{\mathrm{L}_1}(\nabla^*\cdot\mathbf{Q})\cdot(\nabla^*\mathbf{Q})^{\mathrm{T}}\right]\end{aligned} \tag{27}$$

where

$$\tilde{\mathbf{t}}^{\mathrm{t}} = \frac{\mathrm{t}^{\mathrm{t}}}{\mathrm{ckT}^*}, \quad v_1^* = \frac{v_1 6\mathrm{D}_{\mathrm{r}}}{\mathrm{ckT}^*}, \quad v_2^* = \frac{v_2 6\mathrm{D}_{\mathrm{r}}}{\mathrm{ckT}^*}, \quad v_4^* = \frac{v_4 6\mathrm{D}_{\mathrm{r}}}{\mathrm{ckT}^*} \tag{28a, b, c, d}$$

Thus the total dimensionless stress tensor in Equation (21) is neither symmetric nor traceless:

$$\tilde{\mathbf{t}}^{\mathrm{t}} = \begin{bmatrix} \tilde{\mathrm{t}}_{\mathrm{xx}} & \tilde{\mathrm{t}}_{\mathrm{xy}} & \tilde{\mathrm{t}}_{\mathrm{xz}} \\ \tilde{\mathrm{t}}_{\mathrm{yx}} & \tilde{\mathrm{t}}_{\mathrm{yy}} & \tilde{\mathrm{t}}_{\mathrm{yz}} \\ \tilde{\mathrm{t}}_{\mathrm{zx}} & \tilde{\mathrm{t}}_{\mathrm{zy}} & \tilde{\mathrm{t}}_{\mathrm{zz}} \end{bmatrix} \tag{29}$$

The dimensionless first normal stress difference (N_1) and the dimensionless apparent shear viscosity (η) used to characterize the steady shear rheological material functions are given by

$$N_1 = \tilde{t}_{xx} - \tilde{t}_{yy} = \frac{t_{xx} - t_{yy}}{ckT^*}, \quad \eta = \frac{t_{yx}}{\dot{\gamma}} \cdot \frac{6Dr}{ckT^*} \tag{30a,b}$$

PROJECTION OF THE LANDAU-DE GENNES THEORY ONTO THE LESLIE-ERICKSEN THEORY AND RHEOLOGICAL MATERIAL FUNCTIONS

The most successful and established theory applicable to uniaxial nematic flows is that of Leslie and Ericksen (LE) [19]. This theory neglects the short-range order elasticity, and hence it is unable to describe the changes of the scalar order parameter due to the imposition of sufficiently strong flow. Consequently, in this theory, the microstructure is described by the director **n** and the scalar order parameter S is assumed to remain constant, that is, unaffected by the flow, and always equal to its value of equilibrium, $S = S_{eq}$, while the biaxial order parameter P is equal to zero. The total extra-stress tensor $\mathbf{t}^t$ and the director balance equation in the L-E theory [19] are

$$\begin{aligned} \mathbf{t}^t &= p\delta - \frac{\partial f_n}{(\partial \nabla \mathbf{n})^T} \cdot \nabla \mathbf{n} + \alpha_1 \mathbf{A} : \mathbf{nnnn} + \alpha_2 \mathbf{nN} + \alpha_3 \mathbf{Nn} + \alpha_4 \mathbf{A} \\ &\quad + \alpha_5 \mathbf{nn} \cdot \mathbf{A} + \alpha_6 \mathbf{A} \cdot \mathbf{nn} \\ 0 &= \Gamma^e + \Gamma^v \end{aligned} \tag{31}$$

$$\Gamma^e = -\mathbf{n} \times \left(\frac{\partial f_n}{\partial \mathbf{n}} - \nabla \cdot \frac{\partial f_n}{(\partial \nabla \mathbf{n})} \right); \quad \Gamma^v = -\mathbf{n} \times (\gamma_1 \mathbf{N} + \gamma_2 \mathbf{A} \cdot \mathbf{n}) \tag{32a,b}$$

$$\gamma_1 = \alpha_3 - \alpha_2; \quad \gamma_2 = \alpha_6 - \alpha_5 \tag{33a,b}$$

where f_n is the Frank long-range energy density, given in terms of the following splay (K_{11}), twist (K_{22}), and bend (K_{33}) modes:

$$2F = K_{11}(\nabla \cdot \mathbf{n})^2 + K_{22}(\mathbf{n} \cdot \nabla \times \mathbf{n})^2 + K_{33}|\mathbf{n} \times \nabla \times \mathbf{n}|^2 \tag{34}$$

A is the rate of deformation tensor and **N** is the Jaumann derivative of the director **n**:

$$\mathbf{N} = \dot{\mathbf{n}} - \mathbf{n} \cdot \mathbf{W} \tag{35}$$

$\{\alpha_i\}, \quad i = 1, 6$ are the six Leslie viscosities coefficients, where only five of these are independent due to the Parodi's relation [1]:

$$\alpha_6 - \alpha_5 = \alpha_2 + \alpha_3 \tag{36}$$

In this theory the reactive parameter λ that controls flow alignment is given by

$$\lambda = -\frac{\gamma_2}{\gamma_1} = -\frac{\alpha_2 + \alpha_3}{\alpha_3 - \alpha_2} \tag{37}$$

To assure the compatibility of the tensor theory with the Leslie-Ericksen theory we can express the second-order parameter tensor $\mathbf{Q}$ in terms of orthogonal eigenvectors ($\mathbf{n}$, $\mathbf{m}$, and $\mathbf{l}$) and eigenvalues λ_n, λ_m, and λ_l given in Equation (3). The tensor theory is reduced to the LE vector theory that describes the microstructures of the uniaxial phase by imposing

$$\mathbf{Q} = \mathrm{S}\left(\mathbf{nn} - \frac{1}{3}\delta\right); \quad \hat{\mathbf{Q}} = \mathrm{S}(\mathbf{nN} + \mathbf{Nn}) \tag{38a,b}$$

in Equation (31) and comparing the projected results term by term. It should be noted that the form of the Landau-de Gennes theory used here leads to a restricted form of the LE theory since the uniaxial restriction leads to:

$$\mathrm{L}_1 = \frac{\mathrm{K}_{22}}{2\mathrm{S}^2} \quad \mathrm{L}_2 = \frac{\mathrm{K} - \mathrm{K}_{22}}{\mathrm{S}^2} \tag{39}$$

with $\mathrm{K} = \mathrm{K}_{11} = \mathrm{K}_{33}$—that is, the splay and bend modulus are equal. To break the splay-bend equality higher order terms to Equation (7) must be included. The expressions of the Leslie viscosities (A1) in terms of the Landau-de Gennes parameters that result from the projection are given in the Appendix.

The anisotropy of liquid crystals leads to numerous viscosity coefficients in order to describe the flow properties. They strongly depend on temperature and are sensitive to molecular structure [20]. A number of signatures that define the rheological behavior of DNLCs appear as combinations of the various coefficients, thus narrowing down the degrees of freedom. Here we briefly characterize the following signatures: (a) the reactive parameter in Equation (37), (b) the Leslie angle, (c) the Miesowicsz shear viscosities, (d) flow-alignment viscosity, (e) first normal stress difference, and (f) steady shear viscosity.

Reactive Parameter

The qualitative flow behavior of a nematic liquid crystal depends on the sign and magnitude of the reactive parameter or equivalently in the Leslie viscosity coefficients α_2 and α_3. When shearing a nematic liquid crystal two different types of flow behavior are possible, depending on the signs of α_2 and α_3. For disklike molecules, α_3 is always positive, while α_2 can be positive for flow alignment systems ($\lambda < -1$) or negative for nonalignment

systems [7] ($-1 < \lambda < 0$). With equations (A1) we find that the dependence of the reactive parameter λ as a function of the uniaxial order parameter is

$$\lambda = \frac{\beta\left(4 + 2S - S^2\right)}{6S} \tag{40}$$

Figure 2(a) shows the tumbling function λ as a function of the scalar order parameter S for a typical discotic nematic liquid crystal, for different values of β. The tumbling function diverges as S approaches 0. Steady states are only possible when $\lambda < -1$. In the simple aligning disklike nematic, the director reaches a steady-state orientation in shear start-up for all the values of shear rate.

Flow-Alignment Leslie Angle

The flow-alignment angle is known as the Leslie angle θ_{al} and for DNLCs exists for $\lambda < -1$. For shear-aligning discotics flow tends to align the average molecular unit normals along the velocity gradient direction. The alignment angle of the director with the flow direction is positive (2nd quadrant) (Figure 3). For this case, in the shear flow the director lies in the shear-plane and encloses the angle (flow-alignment angle) with x-direction (Figure 3)

$$\cos 2\theta_{al} = \frac{1}{\lambda} \tag{41}$$

Using Equation (A1) we find that the Leslie angle is given by

$$\cos 2\theta_{al} = \frac{6S}{\beta\left(4 + 2S - S^2\right)} \tag{42}$$

The expression in Equation (42) contains only the scalar order parameter S because the simulations from this article have been done for a range of values of the Ericksen number and energy ratio R corresponding to orientation-dominated rheology in which $S \cong S_{eq}$ and $P \cong 0$ [10].

Figure 2(b) shows the alignment angle for disklike molecules as function of the nematic potential U for different values of β (the angle is defined only for flow alignment systems).

Miesowicz Shear Viscosities

Since the shear viscosity of liquid crystals depends on the orientation of **n** with respect to the flow direction, the viscous anisotropy is characterized by three shear viscosities known as the three Miesowicz shear viscosities, shown in Figure 4. These viscosities are obtained under steady simple

a)

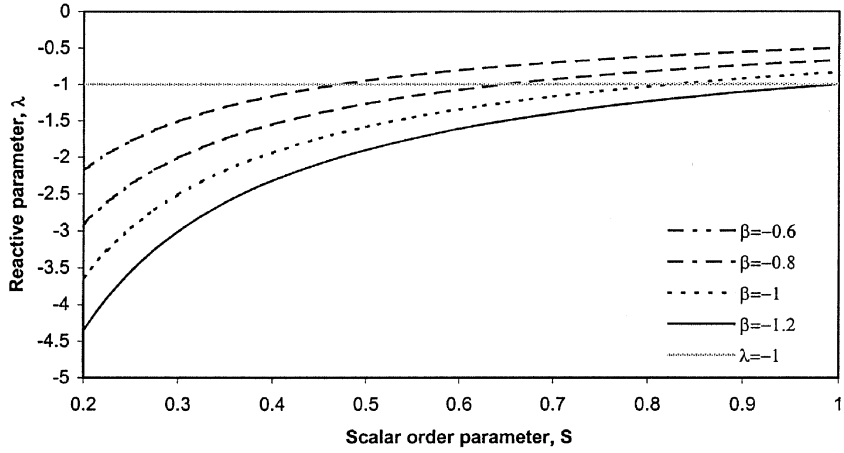

b)

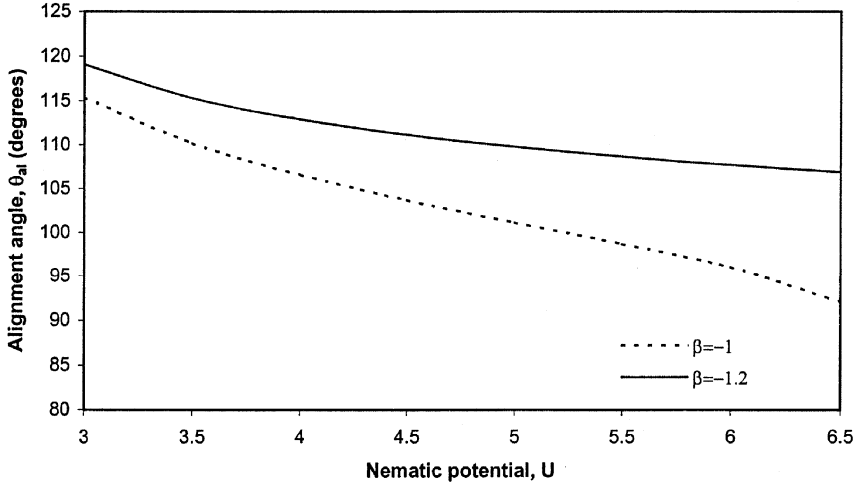

FIGURE 2 (a) The tumbling parameter λ as a function of the scalar order parameter S, for a typical discotic nematic liquid crystal. The tumbling function diverges as S approaches 0. Steady states are only possible when $\lambda < -1$. (b) The alignment angle for disklike molecules as function of U for different β (the angle is defined only for flow alignment systems).

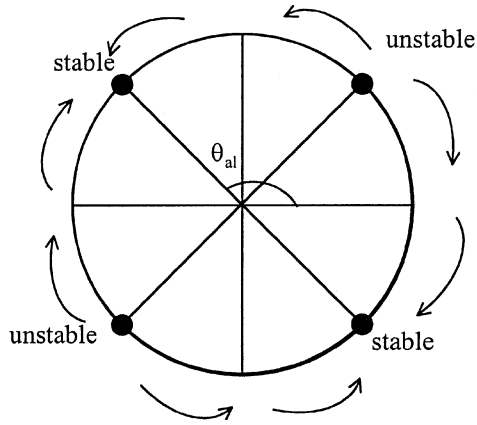

FIGURE 3 Schematic showing the orientation unit circle, with the arrows indicating the directions of rotation imposed by viscous torques, and the stable and unstable flow-alignment angles of a flow-aligning nematic discotic liquid crystal, indicated by the dots, in a steady shearing flow.

shear flow between parallel plates with a fixed director. In terms of the Leslie viscosities they are given by

$$\eta_1 = \frac{1}{2}(\alpha_4 + \alpha_6 + \alpha_3), \quad \eta_2 = \frac{1}{2}(\alpha_4 + \alpha_5 - \alpha_2), \quad \eta_3 = \frac{1}{2}\alpha_4 \qquad (43a,b,c)$$

With the Equations (A1) we find that the dependence of the Miesowicz viscosities as a function of the uniaxial order parameter S is

$$\eta_1(S) = \frac{1}{2}\bar{\eta}\left(v_1^* - \frac{1}{3}v_2^* S + \frac{1}{3}v_4^* S^2 - \frac{2}{3}\beta S\left(2 + S^2 - \frac{S^2}{2}\right) + S^2 + \frac{4}{9}\beta^2\left(1 - S - \frac{S^2}{4}\right) + \frac{1}{3}\beta^2 S\left(4 - S - S^2\right)\right)$$

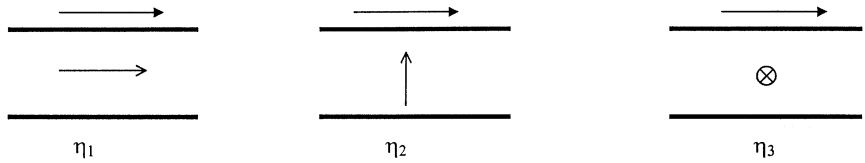

FIGURE 4 The miesowicz viscosities, corresponding to the orientation of the director along one of the three axes: η_1 for the director along the flow direction, η_2 for the director along the velocity gradient direction, and η_3 for the vorticity axis. For discotic nematics the following inequalities hold: $\eta_1 > \eta_3 > \eta_2$.

$$\eta_2(S) = \frac{1}{2}\bar{\eta}\left(v_1^* + \frac{1}{3}v_2^* S + \frac{1}{3}v_4^* S^2 + \frac{2}{3}\beta S\left(2 + S^2 - \frac{S^2}{2}\right) + S^2 + \frac{4}{9}\beta^2\left(1 - S - \frac{S^2}{4}\right) + \frac{1}{3}\beta^2 S\left(4 - S - S^2\right)\right)$$
$$\eta_3(S) = \frac{1}{2}\bar{\eta}\left(v_1^* - \frac{2}{3}v_2^* S + \frac{1}{3}v_4^* S^2 + \frac{4}{9}\beta^2\left(1 - S - \frac{S^2}{4}\right)\right) \quad (44)$$

where $\bar{\eta} = \frac{ckT^*}{6D_r}$. Below we use the dimensionless Miesowicz viscosities obtained by scaling with $\bar{\eta}$.

Flow-Alignment Viscosity

Under shear flow alignment condition the director is given by $\theta = \theta_{al}$, and using Equations (A1) we find that the corresponding steady shear viscosity is

$$\eta_{al} = \frac{1}{2}(\eta_1 + \eta_2 - \gamma_1) + \frac{1}{4}\alpha_1\left(1 - \left(\frac{1}{\lambda}\right)^2\right) \quad (45)$$

which in terms of the scalar order parameter is

$$\eta_{al} = \left(v_1^* + \frac{1}{3}v_4^* S^2 + \frac{4}{9}\beta^2\left(1 - S - \frac{S^2}{4}\right) + \frac{1}{3}\beta^2 S\left(4 - S - S^2\right)\right) + \frac{\left(\frac{v_4^* S^2}{2} - \frac{\beta^2 S^2}{2}\left(\frac{8}{9} - \frac{8}{9}S + \frac{S^2}{12}\right)\right)\left(\beta^2\left(2 + S - \frac{1}{2}S^2\right)^2 - 9S^2\right)}{\beta^2\left(2 + S - \frac{1}{2}S^2\right)^2} \quad (46)$$

For the values of Er and R used in this paper, biaxiality is negligible, as confirmed the numerical calculations.

First Normal Stress Difference

The first normal stress difference N_1 is a characteristic feature of non-Newtonian materials. For nematic liquid crystals N_1 is a strong function of orientation and can have positive or negative values [21]. Expressions for N_1 in terms of the director components n_x and n_y are

$$N_1 = t_{xx} - t_{yy} = \dot{\gamma} n_x n_y (\gamma_2 + \alpha_1(n_y^2 - n_x^2))$$
$$N_1(S) = \dot{\gamma}\bar{\eta} n_x n_y\left(-\frac{2\beta S}{3}\left(2 + S - \frac{1}{2}S^2\right) + \left(2v_4^* S^2 - \beta^2 S^2\left(\frac{8}{9} - \frac{8}{9}S + \frac{S^2}{12}\right)\right)(n_y^2 - n_x^2)\right) \quad (47a,b)$$

which show that orientation along the flow or velocity gradient lead to vanishing normal stress difference. The dimensionless expressions for the first normal stress difference are given by

$$N_1 = \frac{N_1(S)}{ckT^*} \tag{48}$$

For weak flows, we thus expect that the solutions to the L-E theory will also provide a good fit to experimental data, well-characterized boundary conditions, and monodomain initial conditions.

VISCOSITIES COEFFICIENTS SELECTION PROCEDURE

The objective of this section is to formulate and use a selection procedure partially based on the previous section to determine the characteristic parametric values for DNLCs that appear in Equation (31). In order to determine these values, we use the following criteria:

1. Requiring the entropy production to be positive, the following thermodynamic inequalities [1] must be satisfied:

$$\begin{aligned} &\alpha_4 \geq 0 \\ &2\alpha_1 + 3\alpha_4 + 2\alpha_5 + 2\alpha_6 \geq 0 \\ &2\alpha_4 + \alpha_5 + \alpha_6 \geq 0 \\ &4\gamma_1(2\alpha_4 + \alpha_5 + \alpha_6) \geq (\alpha_2 + \alpha_3 + \gamma_2)^2 \end{aligned} \tag{49a,b,c,d}$$

2. Ordering of the Miesowicz shear viscosities:

For the rodlike molecules the following ordering of the three shear Miesowicz viscosities for rods is well established experimentally and theoretically [22]: $\eta_1 < \eta_3 < \eta_2$. Discotic nematics have the following reversed ordering of the Miesowicz viscosities: $\eta_2 < \eta_3 < \eta_1$.

3. The behavior of the first normal stress difference: N_1 normally changes of sign, as predicted by [11] and as measured by Cato et al. [23].

A set of material parameters used in this paper that satisfies all of these theoretical and experimental criteria are: $\nu_1^* = 1$, $\nu_2^* = -1$, and $\nu_4^* > 0$.

RHEOLOGICAL MATERIAL FUNCTIONS

In this section we characterize the influence of (U, β) on the first normal stress difference N_1 in Equation (47) and on the three Miesowicz viscosities in Equation (44).

Figure 5 shows the signs of the dimensionless first normal stress difference N_1 as a function of director angle θ, for (a) $\beta = -1$, $U = 4$, and (a) $v_4^* = 6$ and (b) $v_4^* = 0.5$. The azimuthal coordinate corresponds to the director angle and the radial coordinate to the dimensionless first normal stress difference N_1. The figures shows that the number of sign changes in N_1 is a function of the nonlinear coefficient v_4^*. Figure 6 shows the dimensionless first normal stress N_1 as a function of director orientation θ, for $U = 4$, and increasing v_4^*. The figure shows that N_1 is a periodic function of θ, and that amplitude and frequency increase with v_4^*.

Figure 7(a) shows the dimensionless first normal stress difference N_1 as a function of director orientation θ, for $U = 4$, $v_1^* = 1$, $v_2^* = -1$, $v_4^* = 6$, and increasing β. When β increases, the first normal stress difference is increasing. For all N_1 vanishes at $\theta = 0,\ \pi/2,\ \pi$, and $3\pi/2$. The parameter β changes the coordinates of the additional coordinates corresponding to $N_1 = 0$ that lie between these fixed points. Figure 7(b) shows the dimensionless first normal stress difference N_1 as a function of director orientation θ, for $v_1^* = 1,\ v_2^* = -1,\ v_4^* = 6,\ U = 4,\ U = 5.5$. We can see that increasing the temperature only decreases the amplitude of N_1.

SELECTED COMPUTATIONAL RESULTS

Numerical Procedure

We consider the following three anchoring conditions that correspond to the three Miesowicz orientations (see Figure 4).

1. The director $\mathbf{n}$ is fixed along the flow direction (BC1):

$$\mathbf{n}_1 = (n_x, n_y, n_z) = (1, 0, 0) \tag{50}$$

2. The director $\mathbf{n}$ is fixed along the velocity gradient direction (BC2):

$$\mathbf{n}_2 = (n_x, n_y, n_z) = (0, 1, 0) \tag{51}$$

3. The director $\mathbf{n}$ is fixed along the vorticity direction (BC3):

$$\mathbf{n}_3 = (n_x, n_y, n_z) = (0, 0, 1) \tag{52}$$

The relation between the director components and spherical coordinates are given by (Figure 8b):

$$\mathbf{n}_x = \cos\theta, \quad \mathbf{n}_y = \sin\theta\cos\phi, \quad \mathbf{n}_z = \sin\theta\sin\phi \tag{53a,b,c}$$

where θ is the tilt angle and ϕ is the twist angle. Inplane orientation corresponds to $\phi = 0$, and out-of-plane orientation corresponds to $\phi \neq 0$. At

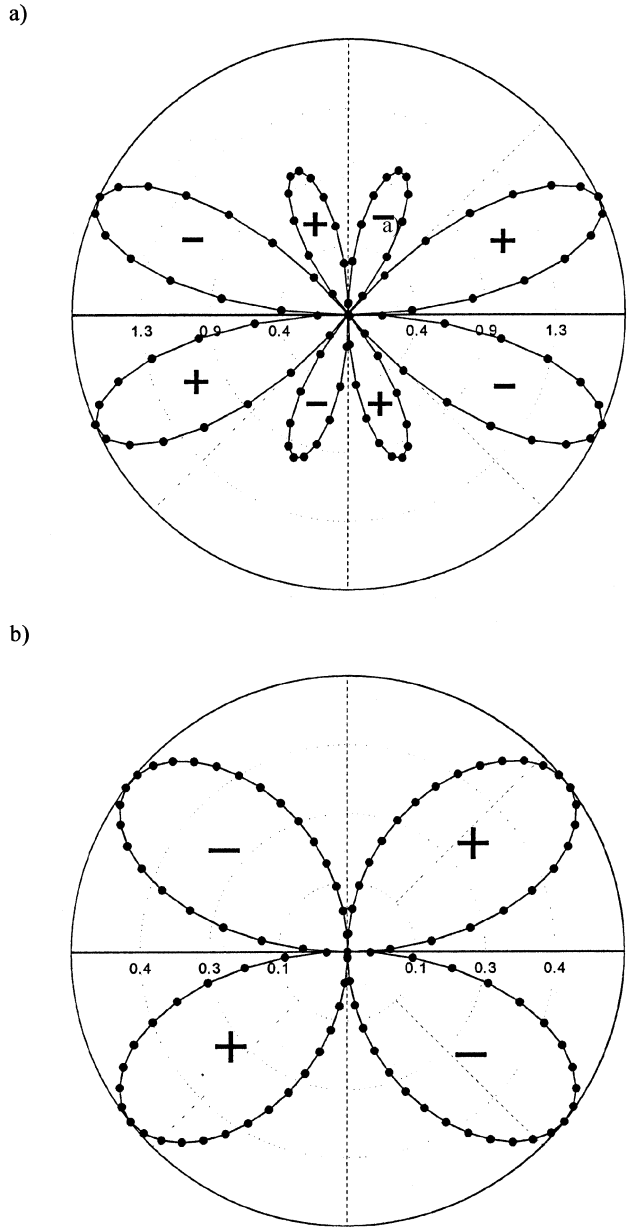

FIGURE 5 Dimensionless first normal stress difference N_1 as a function of director angle θ, for $\beta = -1$, $U = 4$, and $v_4^* = 6$ (a) and $v_4^* = 0.5$ (b). The azimuthal coordinate corresponds to the director angle and the radial coordinate to N_1. The figures show that the number of sign changes in N_1 is a function of the nonlinear coefficient v_4^*.

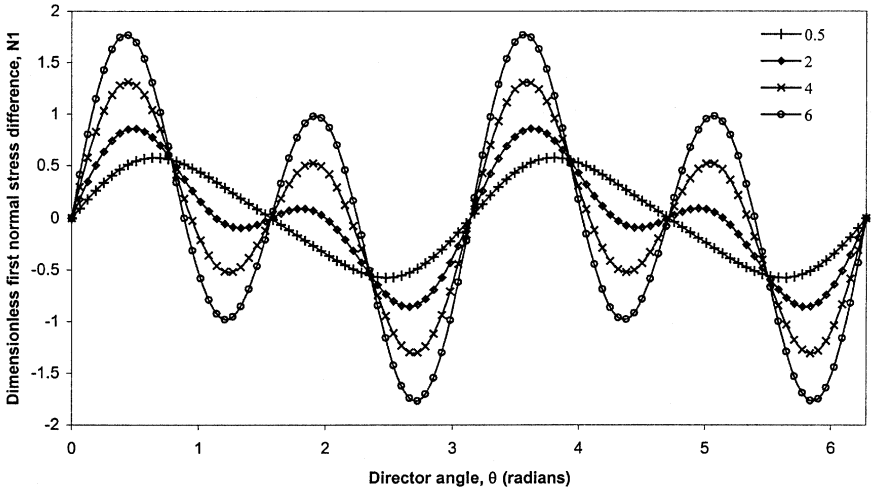

FIGURE 6 The dimensionless first normal stress difference N_1 as a function of director orientation θ, for $U = 4$, and increasing v_4^*. We can see that N_1 is a periodic function of θ, and that amplitude and frequency increase with v_4^*.

the bounding surfaces the discotics are uniaxial ($P = 0$) at equilibrium $S = S_{eq}$:

$$S_{eq} = \frac{1}{4} + \frac{3}{4}\sqrt{1 - \frac{8}{3U}} \tag{54a,b}$$

$$\mathbf{Q}_s(y^* = 0) = \mathbf{Q}_s(y^* = 1) = S_{eq}\left(\mathbf{n}_s\mathbf{n}_s - \frac{\mathbf{I}}{3}\right) \tag{55}$$

The initial state is assumed to be uniaxial and at equilibrium. The orientation of molecules at $t = 0$ is assumed to be parallel to the corresponding orientation $\mathbf{n}_s$, with small thermal fluctuations imposed by introducing infinitesimally small Gaussian noise:

$$\mathbf{Q}(t^* = 0, 0 < y^* < 1) = S_{eq}\left(\mathbf{n}_I\mathbf{n}_I - \frac{\mathbf{I}}{3}\right) \tag{56}$$

We assume that the flow field is known:

$$\mathbf{V} = (y^*V, 0, 0) \tag{57}$$

The simulations are 1D in the velocity gradient direction. The equation set in Equation (6) is solved numerically by using the Galerkin finite element method for spatial discretization [14]. The resulting set of nonlinear time-dependent ordinary differential, obtained after spatial discretization, is

a)

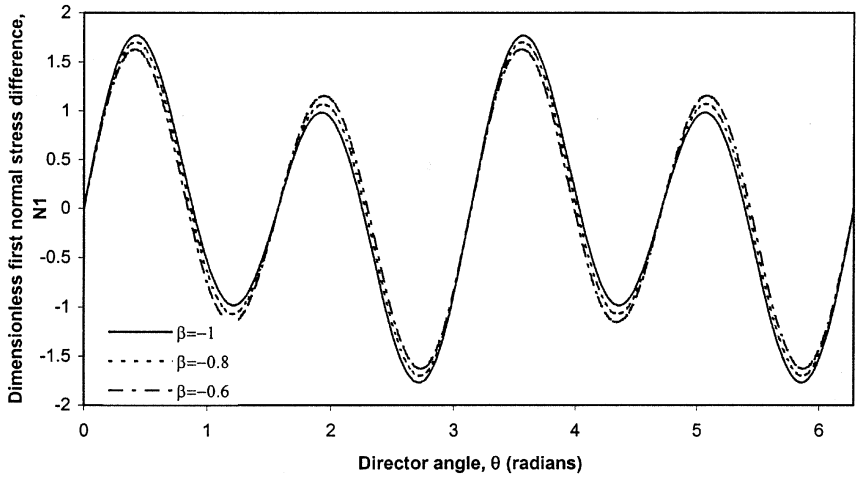

b)

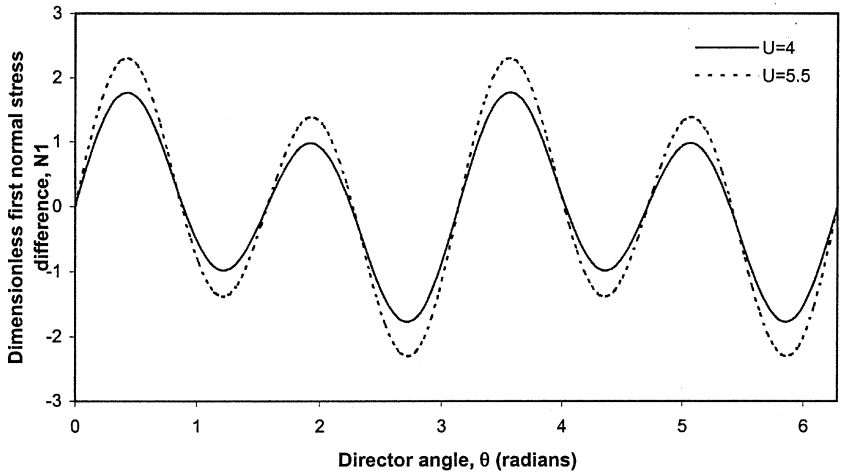

FIGURE 7 (a) The dimensionless first normal stress difference N_1 as a function of director orientation θ, for $U = 4$, $v_1^* = 1$, $v_2^* = -1$, $v_4^* = 6$, and increasing β. When β increases, the first normal stress difference is increasing. For all cases N_1 vanishes at $\theta = 0$, $\pi/2$, π, and $3\pi/2$. The parameter β changes the coordinates of the additional angles corresponding to $N_1 = 0$ that lie between these fixed points. (b) The dimensionless first normal stress difference N_1 as a function of director orientation θ, for $v_1^* = 1$, $v_2^* = -1$, $v_4^* = 6$, and $\beta = -1$ for $U = 4$ and $U = 5.5$. We can see that increasing the temperature only decreases the amplitude of N_1.

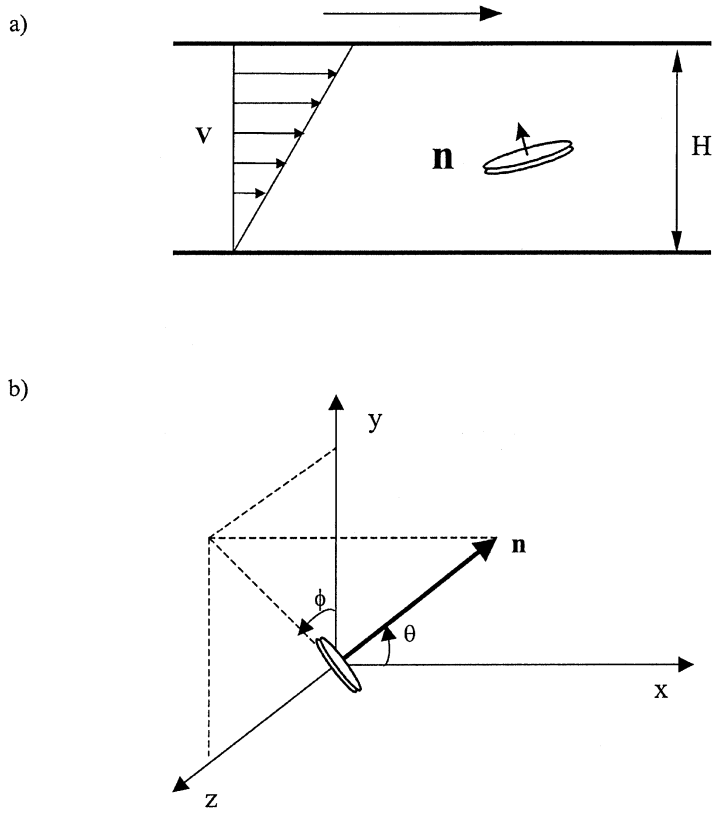

FIGURE 8 Definition of the flow geometry and coordinates system for simple shear flow. (a) The lower plate is at rest and the upper plate moves in the x-direction with a constant velocity V. H is the gap separation. (b) Cartesian coordinate system with x = flow direction, y = the velocity gradient direction, and z = the vorticity axis. The director **n** is defined by the tilt angle θ and the twist angle ϕ.

solved using the Newton-Raphson iteration scheme. The convergence is assumed to occur when the length of the difference between two successive solutions vectors is less than 10^{-6}. A finite difference method is used to discretize time. The simulation parameters are: $U = 4$, $\beta = -1$, $S_{eq} = 0.683$, $v_1^* = 1$, $v_2^* = -1$, $R = 10^5$, $10^{-1} < Er < 10^5$. Under these (R, Er) parametric conditions, the inequalities in Equation (19) ensure that the rheology is under the orientation-control regime. Table 1 gives the calculated values for the Leslie viscosities coefficients for the selected parameters: $U = 4$, $\beta = -1$, $v_1^* = 1$, $v_2^* = -1$, $v_4^* = 0.5$, and $v_4^* = 6$. The theory is consistent with the expected Leslie viscosity parameters for

TABLE 1 Calculated Leslie Coefficients Viscosities, Rotational and Irrotational Viscosities and The Tumbling Parameter for the Parameters Used for the Simulations (U = 4, $\beta = -1$, $v_1^* = 1$, $v_2^* = -1$)

Scaled values $\alpha_i^* = \alpha_i/\bar{\eta}$, $\gamma_i^* = \gamma_i/\bar{\eta}$, $\bar{\eta} = \frac{ckT^*}{6D_r}$	$v_4^* = 0.5$	$v_4^* = 6$
α_1^*	0.316	5.448
α_2^*	0.091	0.091
α_3^*	1.024	1.024
α_4^*	1.550	2.406
α_5^*	−0.591	−0.591
α_6^*	0.523	0.524
γ_1^*	0.933	
γ_2^*	1.115	
λ	−1.195	

DNLCs [7]. Table 2 presents expression and numerical values for the dimensionless rheological material functions used to validate the numerical results. On the first three rows, the alignment angle θ_{al}, the dimensionless first normal stress difference under alignment conditions N_{al}, and the dimensionless alignment shear viscosity η_{al} are shown as a function of S on the left column, and the corresponding numerical values are shown on the right column. On the last three rows the Er = 0 viscosities corresponding to the three boundary conditions in Equations (50), (51), and (52) are shown as a function of S on the left column, and the corresponding numerical values are shown on the right column (the computed Miesowicz viscosities, given by the Equation (43)). As we can see the well-known Hess' ordering of these viscosities is satisfied.

Numerical Results and Discussion

We next discuss the numerical solutions for the following boundary conditions: (a) BC1: $\mathbf{n}(x=0) = \mathbf{n}(x=1) = (1,0,0)$, (b) BC2: $\mathbf{n}(x=0) = \mathbf{n}(x=1) = (0,1,0)$, (c) BC3: $\mathbf{n}(x=0) = \mathbf{n}(x=1) = (0,0,1)$.

Director along the velocity (BC1)

Figure 9 shows the orientation angle θ (solid line) and the scalar order parameter S (points) at the center ($y^* = 0.5$) (a), the dimensionless shear viscosity (b), and the dimensionless first normal stress difference N_1 (c) as a function of the Ericksen number, $v_4^* = 6$ (dotted line), and $v_4^* = 0.5$ (solid line). Figure 9(a) shows that θ has a three-region dependence on Er, a lower and higher plateau, and a power law intermediate region. The high Er plateau corresponds to flow alignment. The numerical results agree with the theoretical results found from Equation (42), which gives

TABLE 2 Rheological Functions Corresponding to the Parameters Used for the Simulations (U = 4, $\beta = -1$, $v_1^* = 1$, $v_2^* = -1$) and for Two Parameters $v_4^* = 0.5$ and $v_4^* = 6$

Relations	$v_4^* = 0.5$	$v_4^* = 6$
$\theta_{al} = \frac{1}{2}\cos^{-1}\frac{6S}{\beta(4+2S-S^2)}$	−73.9 (degrees) or 106.1 (degrees)	
$N_{al} = \frac{Er}{R} n_{xa} n_{ya}\left(-\frac{2\beta S}{3}\left(2+S-\frac{1}{2}S^2\right) + \left(2v_4^* S^2 - \beta^2 S^2\left(\frac{8}{9}-\frac{8}{9}S+\frac{S^2}{12}\right)\right)(n_{ya}^2 - n_{xa}^2)\right)$	−0.0377	0.159
$\eta_{al} = \left(v_1^* + \frac{1}{3}v_4^* S^2 + \frac{4}{9}\beta^2\left(1-S-\frac{S^2}{4}\right) + \frac{1}{3}\beta^2 S(4-S-S^2)\right)$	0.543	1.355
$\frac{\left(\frac{v_4^* S^2}{2} - \frac{\beta^2 S^2}{2}\left(\frac{8}{9}-\frac{8}{9}S+\frac{S^2}{12}\right)\right)\left(\beta^2\left(2+S-\frac{1}{2}S^2\right)-9S^2\right)}{\beta^2\left(2+S-\frac{1}{2}S^2\right)}$		
$\eta_{10} = \frac{1}{2}\left(v_1^* - \frac{1}{3}v_2^* S + \frac{1}{3}v_4^* S^2 - \frac{2}{3}\beta S\left(2+S^2-\frac{S^2}{2}\right) + S^2 + \frac{4}{9}\beta^2\left(1-S-\frac{S^2}{4}\right) + \frac{1}{3}\beta^2 S(4-S-S^2)\right)$	1.562	1.999
$\eta_{20} = \frac{1}{2}\left(v_1^* - \frac{1}{3}v_2^* S + \frac{1}{3}v_4^* S^2 + \frac{2}{3}\beta S\left(2+S^2-\frac{S^2}{2}\right) + S^2 + \frac{4}{9}\beta^2\left(1-S-\frac{S^2}{4}\right) + \frac{1}{3}\beta^2 S(4-S-S^2)\right)$	0.432	0.87
$\eta_{30} = \frac{1}{2}\left(v_1^* - \frac{2}{3}v_2^* S + \frac{1}{3}v_4^* S^2 - \frac{4}{9}\beta^2\left(1-S-\frac{S^2}{4}\right)\right)$	0.778	1.215

The viscosities η_{i0} correspond to the initial state (zero shear viscosity) and the values with the indices "al" correspond to the perfect flow alignment (Er number is 10^5). The values for S correspond to the computed values at $y^* = 0.5$ (n_{xa} and n_{ya} are the director components at the alignment angle).

$\theta_L = -73.9$ degrees. Also we can see that the scalar order parameter is equal with S_{eq} for the values of Ericksen number $Er \ll R$. Figure 9(b) shows that the dimensionless apparent shear viscosity η as a function of Ericksen number displays shear thinning behavior, as predicted by the theory:

$$\eta(Er \to 0) = \eta_{10} = \eta_1 > \eta_{al} \tag{58}$$

That is, at zero Er the viscosity with planar boundary conditions corresponds to the Miesowicz viscosity η_1. The figure shows that the computed

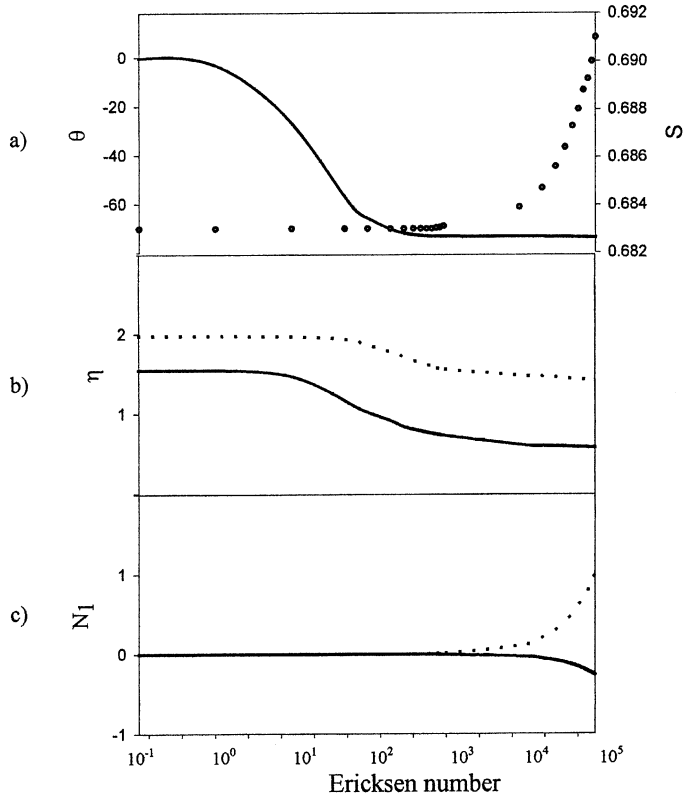

FIGURE 9 (a) Orientation angle and scalar order parameter S at $y^* = 0.5$ for $U = 4$, $\beta = -1$, $L_2^* = -0.3$, and $R = 10^5$. The profiles correspond to the flow-aligning system for boundary conditions BC1. (b) Dimensionless apparent shear viscosity as a function of Ericksen number. (c) Dimensionless first normal stress difference as a function of Ericksen number for $v_4^* = 0.5$ (solid line) and $v_4^* = 6$ (dotted line).

viscosity has low and high Er plateaus, and an intermediate power law shear thinning region. The computed low Er plateau is given by $\eta(\mathrm{Er} = 0) = \eta_{10} = \eta_1$, and the high Er plateau is given by $\eta(\mathrm{Er} = 0) = \eta_{\mathrm{al}}$. The computational values agree with the analytical values. Figure 9(c) shows that the dimensionless first normal stress difference displays a low E_r plateau, eventually followed by a linearly increasing region. For $v_4^* = 0.5$ (solid line) the low Er plateau is followed by a linear region. For $v_4^* = 6$, Figure 10 shows that at very low shear rates the values of N_1 decrease with Er number, followed by increase, and at $\mathrm{Er} = 300$ there is a sign change transition, in agreement with previous results [24]. Thus for this value, N_1 displays a nonmonotonic behavior and a sign change. In partial summary,

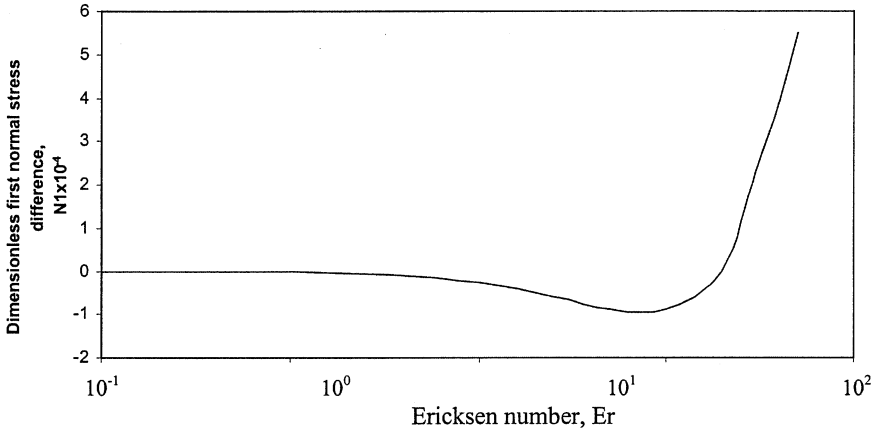

FIGURE 10 Dimensionless first normal stress difference as a function of Ericksen between 0.1 and 500, for boundary conditions BC1, $\mathrm{U}=4$, $\beta=-1$, $\mathrm{L}_2^*=-0.3$, $\mathrm{R}=10^5$, and $v_4^*=6$.

for planar director anchoring the orientation-controlled rheology is characterized by a sign change, from positive to negative as Er increases, in N_1 that corresponds to the power law thinning behavior of the apparent viscosity.

Director Along the Velocity Gradient (BC2)

Figure 11 shows the orientation angle θ (solid line) and the scalar order parameter S (points) at the center ($\mathrm{y}^*=0.5$) (a), the dimensionless shear viscosity (b), and the dimensionless first normal stress difference N_1 (c) as a function of the Ericksen number for boundary condition BC2, $v_4^*=6$ (dotted line), and $v_4^*=0.5$ (solid line). Figure 11(a) shows that θ has a three-region dependence on Er, a lower and higher plateau, and a power law intermediate region. The high Er plateau corresponds to flow alignment. The numerical results agree with the theoretical results found from Equation (42), which gives $\theta_{\mathrm{L}}=106$ degrees. Also we can see that the scalar order parameter is equal with S_{eq} for the values of Ericksen number $\mathrm{Er}\ll\mathrm{R}$. Figure 11(b) shows that the dimensionless apparent shear viscosity η as a function of Ericksen number displays shear thickening behavior, as predicted by the theory:

$$\eta(\mathrm{Er}\to 0)=\eta_{20}=\eta_2<\eta_{\mathrm{al}} \tag{59}$$

That is, at zero Er the viscosity with planar boundary conditions corresponds to the Miesowicz viscosity η_2. The figure shows that the

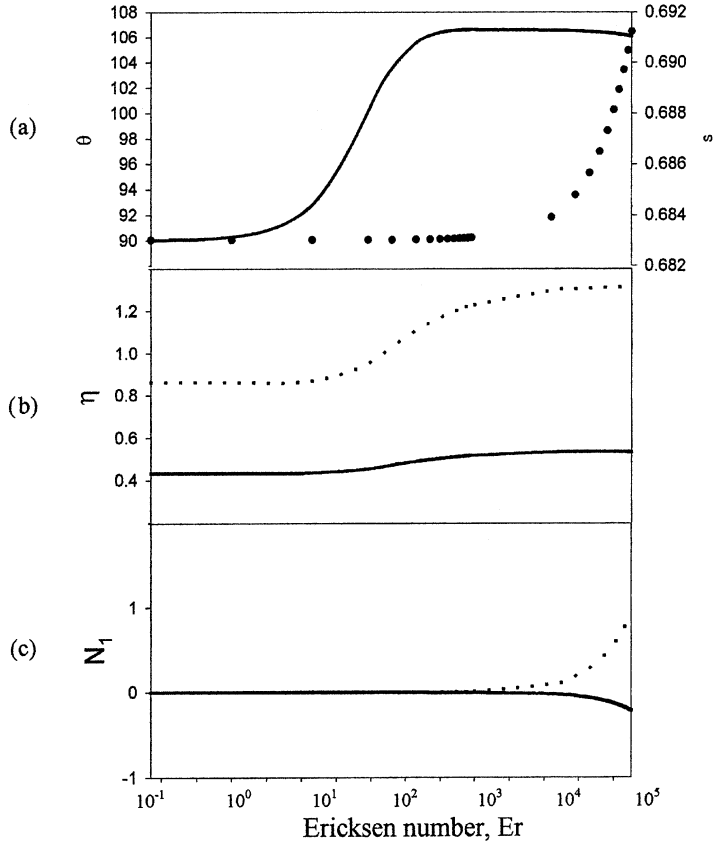

FIGURE 11 (a) Orientation angle and scalar order parameter S at $y^* = 0.5$ for $U = 4$, $\beta = -1$, $L_2^* = -0.3$, and $R = 10^5$. The profiles correspond to the flow-aligning system for boundary conditions BC2. (b) Dimensionless apparent shear viscosity as a function of Ericksen number. (c) Dimensionless first normal stress difference as a function of Ericksen number for $v_4^* = 0.5$ (solid line), and $v_4^* = 6$ (dotted line).

computed viscosity has low and high Er plateaus, and an intermediate power law shear thickening region. The computed low Er plateau is given by $\eta(\mathrm{Er} = 0) = \eta_{20} = \eta_2$, and the high Er plateau is given by $\eta(\mathrm{Er} = 0) = \eta_{\mathrm{al}}$. The computational values agree with the analytical values. Figure 10(c) shows that the dimensionless first normal stress difference displays two regions, a low E_r plateau followed by a linearly increasing region. For $v_4^* = 6$ (dotted line) $N_1 > 0$, and for $v_4^* = 0.5$ (solid line) $N_1 < 0$. The computational results are in perfect agreement with the theoretical results shown on the second row of Table 2. In partial summary, planar

anchoring leads to shear thickening non-Newtonian viscosity behavior. The first normal stress difference can be positive or negative, and after an initial Newtonian plateau its magnitude increases linearly with Er.

Director Along the Vorticity (BC3)

For BC3, experimental data [25] and analytical results [26] show that for low Ericksen number the effect of the boundary conditions along the vorticity promotes the out-of-plane orientation, and further increase in shear rate leads to flow-alignment in the shear plane at a critical shear rate. For the parametric conditions, strong anchoring conditions, and initial conditions used in the present simulations promote the stability of the out-of-plane solution until $\mathrm{Er} = 20$. Figure 12 shows the director angle θ (solid line) and the twist angle ϕ (dotted line) as a function of the dimensionless coordinate y*, for Ericksen number $\mathrm{Er} = 10$ (a), $\mathrm{Er} = 40$ (b), and $\mathrm{Er} = 1000$ (c). Figure 12(a) shows that the director is out of plane, so $\theta = 90$ and $\phi = 90$, while in Figure 12(b) there is only a boundary layer region where the director is out of plane near the bounding surfaces (effect of anchoring boundary conditions), but in the bulk the director is in plane. Figure 12(c) shows that the director is in plane for all values of y* except near to the bounding surfaces.

Figure 13 shows the orientation angle θ (dotted line) and the twist angle ϕ (solid line) (a), the dimensionless shear viscosity (b), and the dimensionless first normal stress difference N_1 (c) as a function of the Ericksen number, for $v_4^* = 6$ (solid line), and $v_4^* = 0.5$ (dotted line). Figure 13(a) shows that θ has a three-region dependence on Er, a lower and higher plateau, and a power law intermediate region. The high Er plateau corresponds to flow alignment. The numerical results agree with the theoretical results found in Equation (39), which gives $\theta_{\mathrm{L}} = 106$ degrees. For the twist angle we have also three regions, for low Er number $\phi = 90$ degrees, a power law intermediate region, and for higher Er numbers $\phi = 0$.

Figure 13(b) shows that the dimensionless apparent shear viscosity η as a function of Ericksen number corresponds to $v_4^* = 6$ (solid line) and $v_4^* = 0.5$ (dotted line). As we expected, the viscosity is constant while the orientation is out of plane and perpendicular on the shear plane. The computed viscosity in this case is exactly equal to the Miesowicz viscosity η_3, although at higher Er numbers the director orients away from the vorticity axis and lies entirely on the shear plane, and the viscosity tends to the alignment value (see Table 2). The viscosity for $v_4^* = 6$ is non-monotonic, and the local minimum corresponds to the out-of-plane→in-plane transition.

Figure 13(c) shows the dimensionless first normal stress difference N_1 as a function of Ericksen number corresponding to the two values of $v_4^* = 6$ (solid line), and $v_4^* = 0.5$ (dotted line). We can see that the values of N_1 are

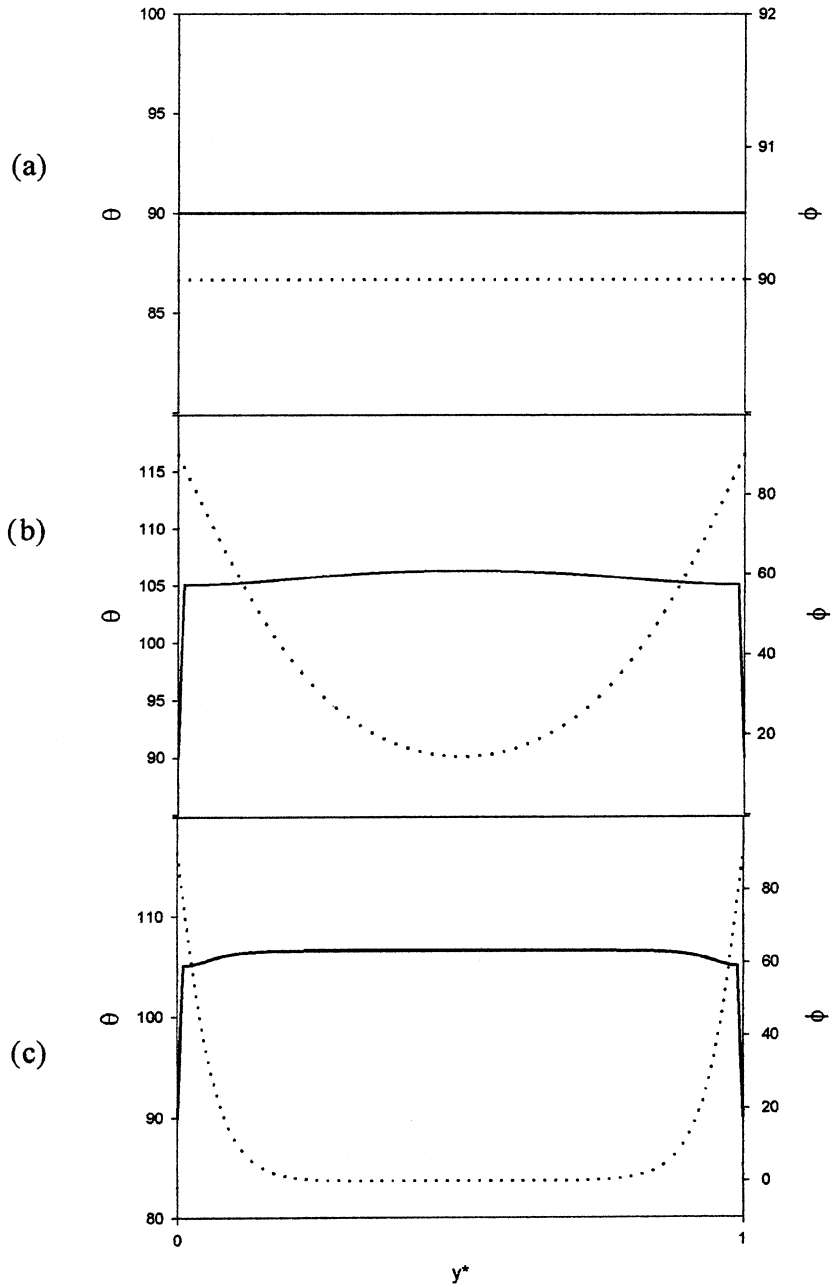

FIGURE 12 Director tilt angle θ (solid line) and the twist angle ϕ (dotted line) function of dimensionless distance y*, for Ericksen number $E_r = 10$ (a), $E_r = 40$ (b), and $E_r = 1000$ (c).

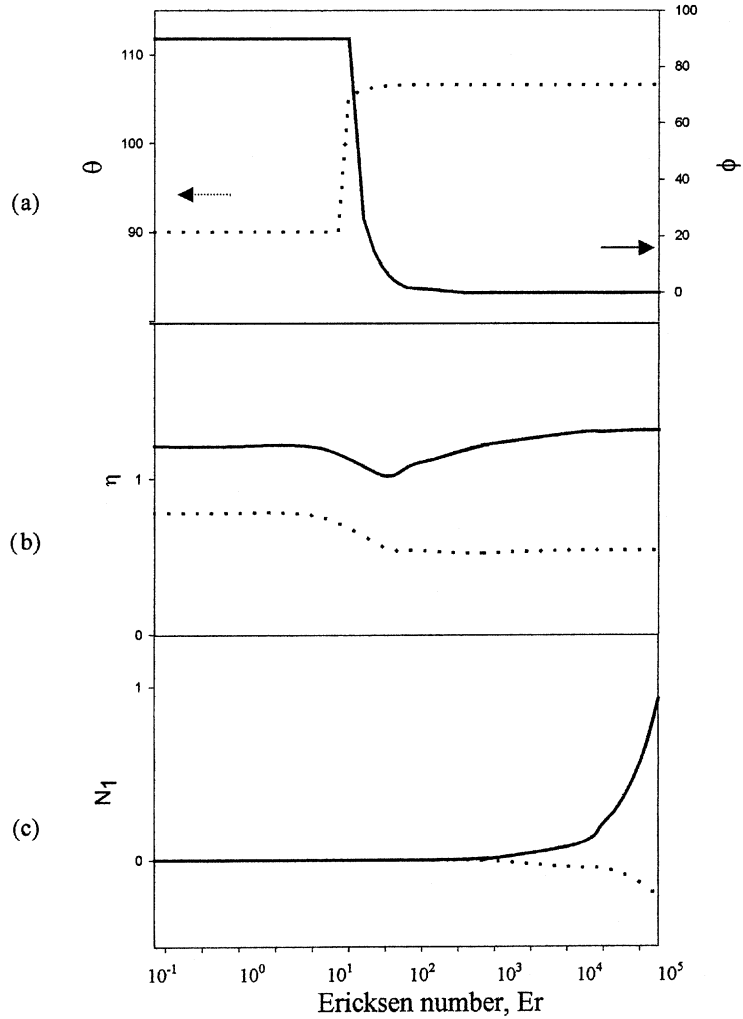

FIGURE 13 (a) Director tilt angle, θ angle, and twist angle at $y^* = 0.5$ for $U = 4$, $\beta = -1$, $L_2^* = 0.3$, and $R = 10^5$. The profiles correspond to the flow-aligning system for boundary conditions BC3. (b) Dimensionless apparent shear viscosity as a function of Ericksen number. (c) Dimensionless first normal stress difference as a function of Ericksen number for $v_4^* = 0.5$ (dotted line), and $v_4^* = 6$ (solid line).

zero when the director is out of plane. Figure 13(c) shows that the dimensionless first normal stress difference displays two regions: a low E_r plateau followed by a linearly increasing region.

Rheological Scaling Laws

The material (η, N_1) functions presented above can be fitted to classical rheological models that contain parameters describing the time constant of the material and a power law exponent.

Viscosity Scaling

The scaled viscosity for DNLCs can be fitted for all boundary conditions as follows:

$$\eta^* = \frac{\eta - \eta_{al}}{\eta_{i0} - \eta_{al}} \quad i = 1, 2, 3 \tag{60}$$

where the subscript "i" denotes the boundary condition (i = 1, BC = BC1, etc.). The classical Carreau-Yasuda model [27], is a three parameter model for a non-Newtonian fluid, which has a good flexibility to fit a wide variety of viscosity as a function of shear rate $\eta(\dot{\gamma})$ flow curves. The Carreau-Yasuda model is given by:

$$\eta^* = \left[1 + (\tau'\dot{\gamma})^a\right]^{\frac{n-1}{a}} \tag{61}$$

where η^* is the scaled shear viscosity, n is the "power-law exponent," a is a dimensionless parameter that describes the transition region between the zero-shear rate region and the power-law region, τ' is a time constant, and $\dot{\gamma}$ is the shear rate. In the present context we can recast this classical model in terms of liquid crystalline physics using the dimensionless Ericksen number. The Carreau-Yasuda liquid crystal model is given by:

$$\eta^* = \frac{\eta - \eta_\infty}{\eta_0 - \eta_\infty} = \left[1 + (\tau \mathrm{Er})^a\right]^{\frac{n-1}{a}} \tag{62}$$

where η_∞ is the infinite shear rate viscosity (in our case the alignment viscosity of alignment), η_0 is the shear rate viscosity (in our case corresponds to the three Miesowicz viscosities, respectively) and τ a dimensionless time constant. The transition region in the Carreau-Yasuda liquid crystal model is defined by Er = 1/a, i.e., the Ericksen number at which flow significantly affects the orientation. We will fix the "power-law" exponent n at 0.5 value, because in the LE theory, in the shear-thinning region, the apparent viscosity scales with $\mathrm{Er}^{-0.5}$ [10]. In order to fit the curves of the scaled apparent viscosity, we have used the Marquardt-Levenberg algorithm. Table 3 shows different coefficients (R, the multiple correlation coefficient and R^2, the coefficient of determination) which are both measures of how well the regression model in Equation (62) describes the simulation data (the values have to be near 1) and the standard error of estimate ε.

Figure 14 shows the scaled viscosity (Equation (62), $\eta_0 = \eta_1$) for BC1 $\nu_4^* = 0.5$ (a) and $\nu_4^* = 6$ (b) (the solid lines are the fitted curves). Figure 15

TABLE 3 The Values of the Multiple Correlation Coefficient R, the Coefficient of Determination R^2, and the Standard Error of Estimate ε for all Boundary Conditions and for Two Values of the Adimensional Viscosity Coefficient ν_4^* (0.5 and 6)

Boundary conditions	ν_4^*	R	R^2	ε
BC1	0.5	0.998	0.997	0.0142
	6	0.998	0.997	0.0148
BC2	0.5	0.994	0.988	0.0338
	6	0.992	0.985	0.0393
BC3	0.5	0.971	0.944	0.1123

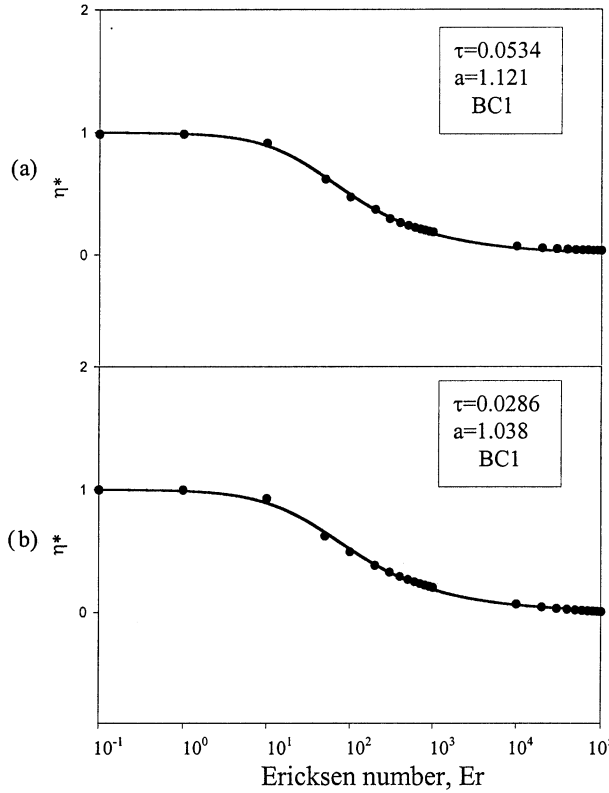

FIGURE 14 The scaled viscosities (Equation (60)) for BC1 (a) $\nu_4^* = 0.5$ and (b) $\nu_4^* = 6$. The solid lines are the fitted curves using Carreau-Yasuda liquid crystal model (Equation (62)). The values for the Carreau-Yasuda model parameters are shown in the figures.

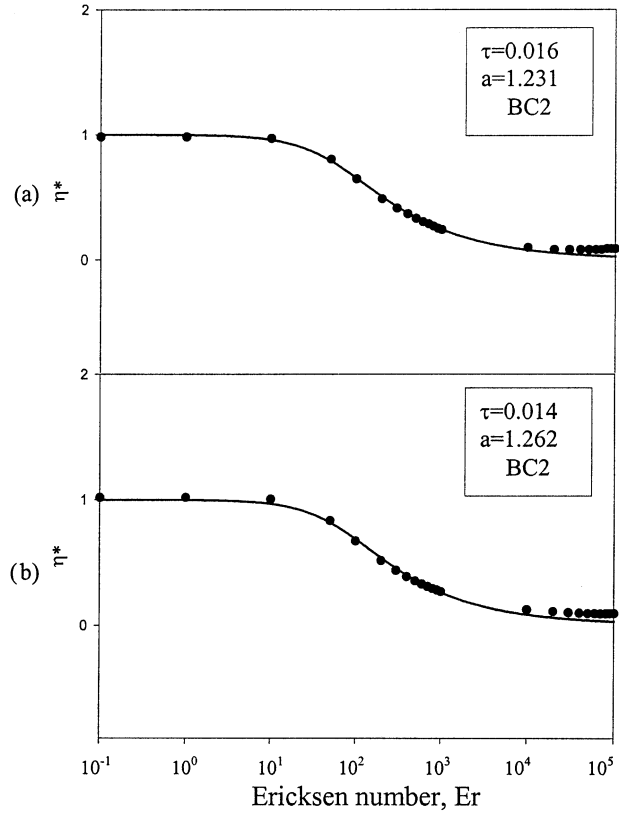

FIGURE 15 The scaled viscosities (Equation (60)) for BC2 (a) $v_4^* = 0.5$ and (b) $v_4^* = 6$. The solid lines are the fitted curves using Carreau-Yasuda liquid crystal model (Equation (62)). The values for the Carreau-Yasuda model parameters are shown in the figures.

shows the scaled viscosities (Equation (62), $\eta_0 = \eta_2$) for BC2 $v_4^* = 0.5$ (a) and $v_4^* = 6$ (b) (the solid lines are the fitted curves and the dots are the computed values). The values for the parameters are shown in the figures. The transition region occurs 1.15 ± 0.112, and the time constant is 0.0337 ± 0.0197. The only significant influence of the boundary conditions is through the value of the transition parameter a. The ordering of the transition parameter, a (BC2) > a (BC1), is due to the fact that the governing torque coefficient for BC2 is α_2 and for BC1 is α_3, and $\alpha_3 \gg \alpha_2$ (see Table 1).

Figure 16 shows the scaled viscosities (Equation (62), $\eta_0 = \eta_3$) for BC3 (a) $v_4^* = 0.5$ and (b)$v_4^* = 6$. In this case BC3 (b) the behavior of the scaled

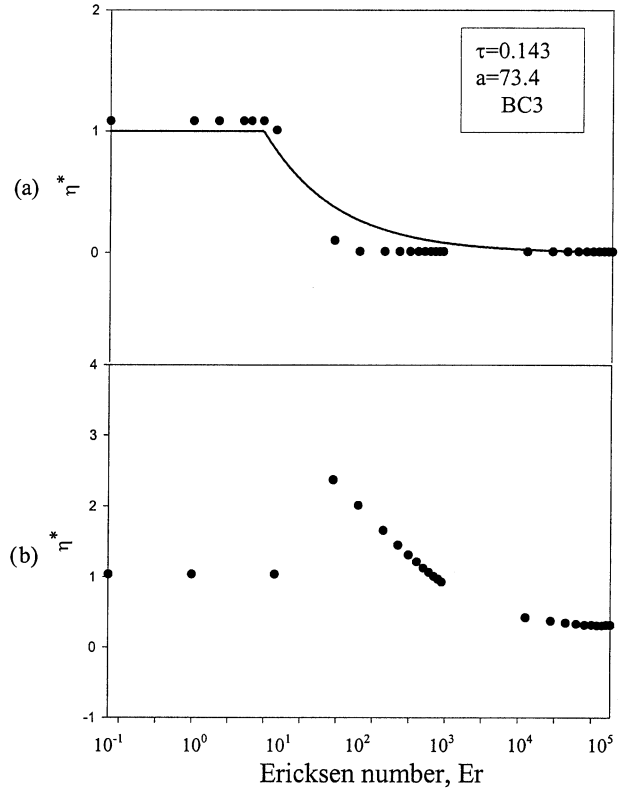

FIGURE 16 The scaled viscosities (Equation (60)) for BC3 (a) $v_4^* = 0.5$ and (b) $v_4^* = 6$.

viscosities are not monotonic, so the Carreau-Yasuda liquid crystal model is not applicable.

The first normal stress can be characterized by a coefficient

$$\Psi = \frac{N_1}{Er} \tag{63}$$

since we know that at higher Er the normal stress grows linearly. An efficient scaling of the first normal stress coefficient is:

$$\Psi^* = \frac{\Psi_\infty - \Psi}{\Psi_\infty} \tag{64}$$

where $\Psi_\infty = \frac{|N_{al}|}{Er}$, where N_{al} is the normal stress in the alignment regime. The values of Ψ_∞ for $v_4^* = 0.5$ is $\Psi_\infty = 0.0377 \cdot 10^{-5}$ and for $v_4^* = 6$ is $\Psi_\infty = 0.159 \cdot 10^{-5}$.

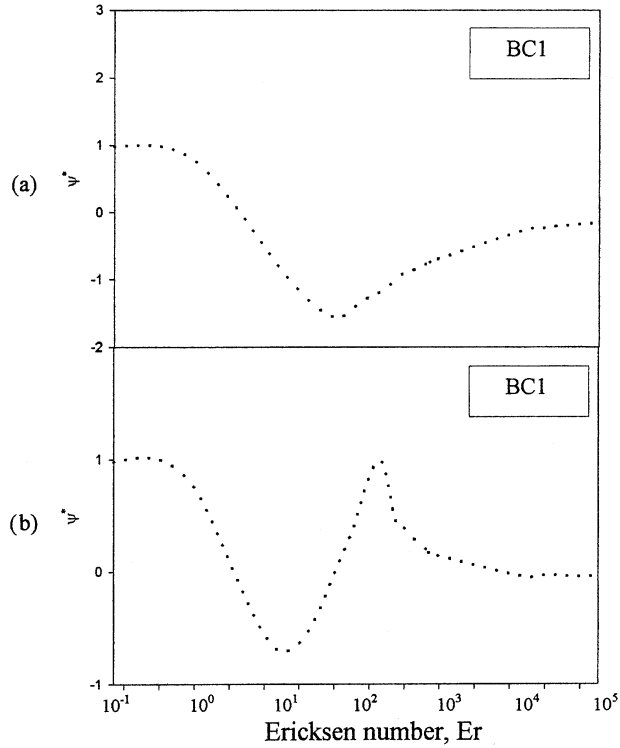

FIGURE 17 The scaled stress coefficients (Equation (64)) for the boundary conditions BC1 (a) $v_4^* = 0$, and (b) $v_4^* = 6$.

Figures 17–19 show the scaled first normal stress coefficient Ψ^* as function of the Ericksen number for all three boundary conditions, BC1 (Figure 17), BC2 (Figure 18), and BC3 (Figure 19), for $v_4^* = 0.5$ (a) and $v_4^* = 6$ (b) (the solid lines are the fitted curves and the dots are the computed values). Figure 17 shows that for BC1, the behavior of the scaled stress coefficient is nonmonotonic. Figures 18 and 19 show that for BC2 and BC3 the scaled normal stress coefficient follows the Carreau-Yasuda liquid crystal model with the power-law exponent of n $\cong$ 0.4. For Figures 18 and 19 we can see three regions: at low Ericksen numbers, the scaled stress coefficient is almost 1; the second region, where we have a power low intermediate region; and at high Ericksen numbers, where the stress coefficient tends to the alignment value $\Psi_{\text{al}} = \frac{|N_{\text{al}}|}{\text{Er}}$, so the scaled stress coefficient will tend to 0. The strong effect of v_4^* on the transition parameter a, shown in Figure 18, is due to the change in α_1.

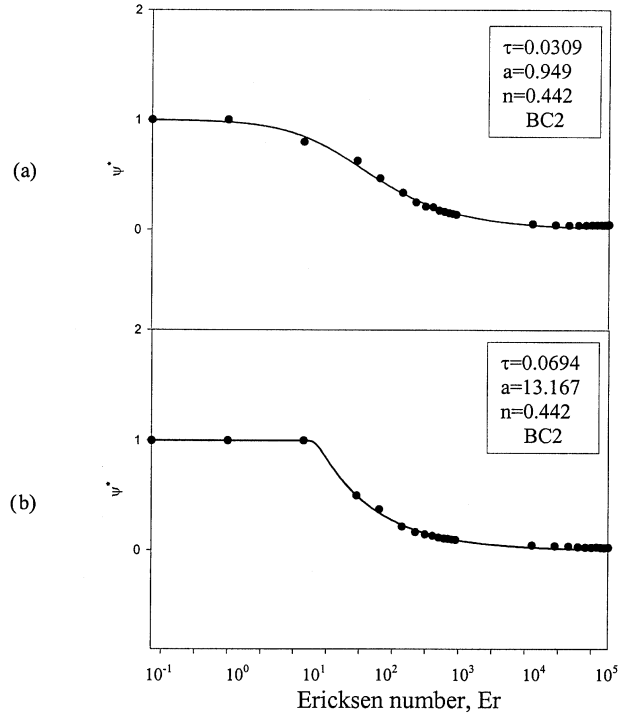

FIGURE 18 The scaled stress coefficients (Equation (64)) for the boundary conditions BC2, (a) $v_4^* = 0$, and (b) $v_4^* = 6$. The solid lines are the fitted curves using Carreau-Yasuda liquid crystal model (Equation (62)). The values for the Carreau-Yasuda model parameters are shown in the figures.

This section has shown that for the scaled viscosity, the Carreau-Yasuda liquid crystal model is always applicable for BC1 and BC2 but may fail for BC3, since in this case the viscosity may be nonmonotonic. On the other hand, the scaled first normal stress coefficient the Carreau-Yasuda liquid crystal model is always applicable for BC2 and BC3, but may fail for BC1 because N_1 maybe nonmonotonic.

CONCLUSIONS

A Landau-de Gennes model that takes into account short-range and long-range energy and flow-induced orientations has been adapted to describe the flow behavior of flow-aligning thermotropic discotic nematic liquid

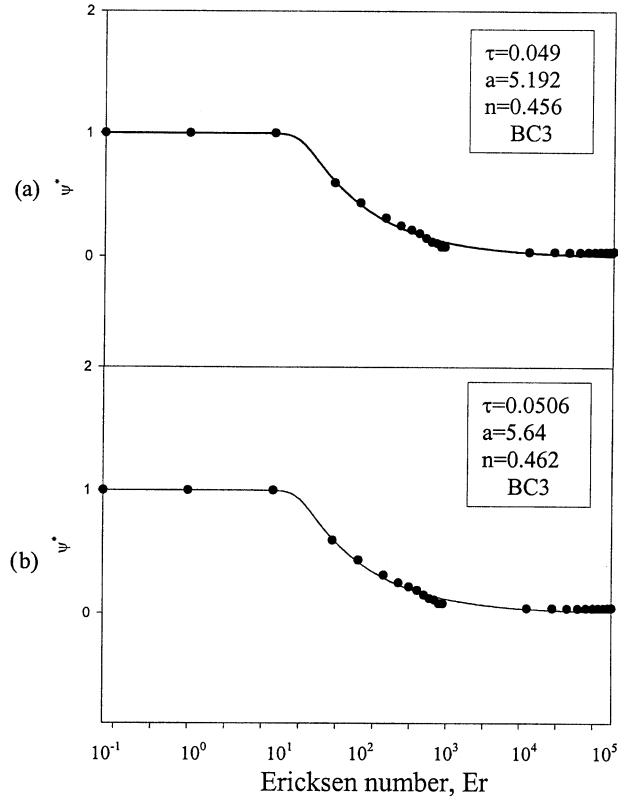

FIGURE 19 The scaled stress coefficients (Equation (64)) for the boundary conditions BC3, (a) $v_4^* = 0$ and (b) $v_4^* = 6$. The solid lines are the fitted curves using Carreau-Yasuda liquid crystal model (Equation (62)). The values for the Carreau-Yasuda model parameters are shown in the figures.

crystals as models of carbonaceous mesophases. The orientation-controlled steady shear rheology of discotic nematic liquid crystals that emerge under the absence of molecular order variations has been characterized by using well-known restrictions of the viscoelastic parameters that enter in the theory, including flow-alignment angle, ordering of the Miesowicz viscosities, and sign changes in first normal stress difference. Theoretical limiting values, valid at infinitesimal and large shear rates, are obtained by projecting the Landau-de Gennes tensor model into the Leslie-Ericksen vectorial equations, and used to validate the numerical results obtained from tensor equations. The rheological response as a function of shear rate is characterized for director anchoring conditions along the flow, the

velocity gradient, and the vorticity directions. Director anchoring along the velocity direction exhibits a strong non-Newtonian rheology, including shear thinning, and nonmonotonic first normal stress difference that includes a sign change with increasing shear rate. Director anchoring along the velocity gradient direction exhibits a strong non-Newtonian rheology, including shear thickening, and a monotonic first normal stress. Director anchoring along the vorticity leads to a strong non-Newtonian rheology, including shear thickening, shear thinning, and a monotonic first normal stress. A new Carreau-Yasuda liquid crystal model has been used to characterize the shear rheology for the three characteristic boundary conditions, and a viscosity power law exponent of 0.5, and a normal stress coefficient power law exponent of 0.44 have been obtained.

REFERENCES

[1] Chandrasekhar, F. R. S. (1992). *Liquid Crystals*. 2nd ed. Cambridge: University Press.
[2] Lewis, I. C. (1978). *Carbon*, *16*(6), 503.
[3] McHugh, J. J., Liu, G. Z., & Edie, D. D. (1992). *Tanso*, *155*, 417.
[4] McHugh, J. J., & Edie, D. D. (1995). *Liq. Cryst.*, *18*, 327.
[5] Sollich, H., Baalss, D., & Hess, S. (1989). *Mol. Cryst. Liq. Cryst.*, *168*, 189.
[6] Tsuji, T., & Rey, A. D. (1997). *JNNFM*, *73*, 127.
[7] Carlsson, T. (1982). *Mol. Cryst. Liq. Cryst.*, *89*, 57.
[8] Han, W. H., & Rey A. D. (1995). *J. Rheol.*, *39*(2), 301.
[9] Larson, R. G., & Mead, D. W. (1992). *Liq. Cryst.*, *12*(5), 751.
[10] Larson, R. G. (1999). *The Structure and Rheology of Complex Fluids*. New York: Oxford University Press.
[11] Currie, P. K. (1981). *Mol. Cryst. Liq. Cryst.*, *73*, 1.
[12] De Gennes, P. G., & Prost, J. (1993). *The Physics of Liquid Crystals*. 2nd ed. London: Oxford University Press.
[13] Singh, A. P., & Rey, A. D. (1998). *Rheologica Acta*, *37*, 374.
[14] Singh, A. P., & Rey, A. D. (2000). *J. Non-Newtonian Fluid Mech.*, *94*, 87.
[15] Farhoudi, Y., & Rey, A. D. (1993). *Rheol Acta*, *32*, 207.
[16] Larson R. G. (1996). *Rheologica Acta*, *35*, 150.
[17] Farhoudi, Y., & Rey, A. D. (1993a). *J. Rheol*, *37*, 289.
[18] Farhoudi, Y., & Rey, A. D. (1993b). *JNNFM*, *49*, 175.
[19] Leslie, F. M. (1979). *Adv. Liq. Cryst*, *4*, 1.
[20] Osipov, M. A., & Terentjev, E. M. (1989). *Z. Naturforsch*, *44A*, 785.
[21] Baalss, D., & Hess, S. (1988). *Z. Naturforsch*, *43A*, 662.
[22] Ehrentrant, H., & Hess, S. (1995). *Phys. Rev. E*, *51*(3), 2203.
[23] Cato, A. D., & Edie, D. (2000). *Eurocarbon*, 15(2000), Berlin, Germany: European Carbon Association.
[24] Cato, A. D., & Edie, D. (2001). *Carbon '01, An International Conference on Carbon, Lexington, KY, United States, July* 14–19, 965.
[25] Pieranski, P., & Guyon, E. *Solid State Communications*, **13**, 435, (1973).
[26] Leslie, F. M. *J. Phys. D : Appl. Phys.*, **9**, 925, (1976).
[27] Bird, R. B., Armstrong, R. C., & Hassenger, O. "*Dynamics of polymeric liquids*", vol. 1, John Wiley & Sons, 169-175, (1987).

APPENDIX

Coefficients of the Leslie-Ericksen Theory

A direct mapping of the Leslie-Ericksen vectorial theory (Equation (31)) with the present model in the absence of the spatial homogenities and for the uniaxial approximation gives the relations for the Leslie viscosities in terms of β and the uniaxial scalar order parameter:

$$
\begin{aligned}
\alpha_1 &= \bar{\eta}\left(2v_4^*\mathrm{S}^2 - \beta^2\mathrm{S}^2\left(\frac{8}{9} - \frac{8}{9}\mathrm{S} + \frac{\mathrm{S}^2}{12}\right)\right)\\
\alpha_2 &= \bar{\eta}\left(-\mathrm{S}^2 - \frac{1}{3}\beta\mathrm{S}\left(2 + \mathrm{S} - \frac{\mathrm{S}^2}{2}\right)\right)\\
\alpha_3 &= \bar{\eta}\left(\mathrm{S}^2 - \frac{1}{3}\beta\mathrm{S}\left(2 + \mathrm{S} - \frac{\mathrm{S}^2}{2}\right)\right)\\
\alpha_4 &= \bar{\eta}\left(v_1^* - \frac{2}{3}v_2^*\mathrm{S} + \frac{1}{3}v_4^*\mathrm{S}^2 + \frac{4}{9}\beta^2\left(1 - \mathrm{S} - \frac{\mathrm{S}^2}{4}\right)\right)\\
\alpha_5 &= \bar{\eta}\left(v_2^*\mathrm{S} + \frac{1}{3}\beta\mathrm{S}\left(2 + \mathrm{S} - \frac{1}{2}\mathrm{S}^2\right) + \frac{1}{3}\beta^2\mathrm{S}\left(4 - \mathrm{S} - \mathrm{S}^2\right)\right)\\
\alpha_6 &= \bar{\eta}\left(v_2^*\mathrm{S} - \frac{1}{3}\beta\mathrm{S}\left(2 + \mathrm{S} - \frac{1}{2}\mathrm{S}^2\right) + \frac{1}{3}\beta^2\mathrm{S}\left(4 - \mathrm{S} - \mathrm{S}^2\right)\right)
\end{aligned}
\tag{A1}
$$